Discover Applied Sciences

Research

Streamflow projections for the Jhelum River basin under climate change

Mustafa Javed[1,2] · **Jürgen Böhner**[3] · **Shabeh ul Hasson**[1]

Received: 31 January 2025 / Accepted: 13 March 2025
Published online: 05 April 2025

Abstract
High Asian mountain water resources, which serve as a lifeline for downstream communities, are vulnerable to warmer future climates. Following the Inter-Sectoral Impact Model Intercomparison Project (ISIMIP) 3b protocol, the future changes in the mean and extreme streamflow of the Jhelum River under the shared socioeconomic pathways (SSPs) of SSP1-2.6, SSP3-7.0, and SSP5-8.5 were quantified. For this, successful calibration and validation of the eco-hydrological Soil and Water Integrated Model (SWIM) against observed streamflow for 1999–2004 and 1994–1999, respectively was completed. Then, the SWIM was forced with bias-adjusted ISIMIP3b historical (1985–2014) and future (2016–2100) datasets. Climate change analysis suggests a warming of 0.9 °C, 5.7 °C, and 7.5 °C per century under SSP1-2.6, SSP3-7.0, and SSP5-8.5, whereas substantial wetting of 329 mm, 665 mm, and 1258 mm per century under SSP1-2.6, SSP3-7.0, and SSP5-8.5, relative to the historical period. Seasonal temperature changes reveal that during the monsoon temperature increase was more pronounced specifically 5.78 °C whereas precipitation also increased markedly 20.84% during the monsoon season for the far future climate under the high-end warming scenario of SSP5-8.5. Subsequently, the mean ensemble changes suggest an increase in low flows (89% in February) but a decrease in high flows (37% in June) under all SSP scenarios, more pronounced under the high-end warming scenario of SSP5-8.5. Further, the 30-year return level will decrease for the near-future (2016–2043), mid-future (2044–2071) and far-future (2072–2100) climates under SSP1-2.6, ranging from −7.01% to −9.87%, under SSP3-7.0, ranging from − 7.22% to − 13.35%, and under SSP5-8.5, ranging from − 9.41% to − 26.60% for the ensemble of five models under consideration which imply a reduction in the likelihood or magnitude of extreme river flow events. The outcomes of this study will advance our knowledge of the discharge dynamics of the Jhelum River Basin under climate change, which will facilitate the better management of precious water resources.

Keywords Streamflow · ISIMIP · SSPs · SWIM · Jhelum River Basin

Supplementary Information The online version contains supplementary material available at https://doi.org/10.1007/s42452-025-06721-y.

✉ Mustafa Javed, mustafa.javed@uni-hamburg.de | [1]HAREME Lab, Institute of Geography, CEN, Universität Hamburg, Hamburg, Germany. [2]Research Department II: Climate Resilience, Potsdam Institute for Climate Impact Research, Potsdam, Germany. [3]Institute of Geography, CEN, Universität Hamburg, Hamburg, Germany.

1 Introduction

On a global scale, during 1880–2012, the average temperature (land and ocean combined) increased by 0.85 °C [1]. This unprecedented global warming is anticipated to escalate in future projections under prominent Representative Concentration Pathway (RCP) scenarios. Global atmospheric changes have triggered unprecedented imbalances in the hydrological cycle [2, 3]. Considering current and projected warming trends, the global hydrological cycle is under great stress. For example, accelerated evapotranspiration rates caused by the rise in global temperature have significantly changed the precipitation dynamics worldwide [4]. Additionally, the changing global mean surface temperature trend and altered rainfall regimes are likely to persist over the coming century [5]. In addition to the changes in the global climate, local and regional climates are also deviating [6, 7]. For instance, several studies have reported increased temperatures over the Himalayan watersheds [8, 9]. Climate change is expected to significantly influence the timing and magnitude of river flows [10, 11].

Rivers are critical for meeting the world's water needs. Specifically, for agrarian economies' rivers play a crucial role in economic development. Humans are affected by variations in flow regimes in terms of water availability for industrial and domestic use, electricity production, and extreme flooding events. Additionally, information about the likely changes in the availability of water is crucial for sustainable development because the region's countries already find it difficult to work together because of limited transboundary water resources. Conflicts may arise due to inefficient use and uneven distribution of water resources in the Himalayan watersheds. The impact of climate change on water resources is a major issue for future development. Therefore, monitoring and management of these precious water resources is crucial in a warming world.

The prediction of future changes especially in the transboundary basins becomes difficult due to the limited number of studies that have examined current and projected climate change and its effects on the water resources. Nevertheless, few studies have reported the impacts of climate change on the water resources of the transboundary Jhelum River Basin (JRB). For instance, Mahmood and Jia [12] assessed the water resources of JRB under the climate change scenarios of HadCM3 where they reported an increase of 10%–15% in the mean annual flow relative to the historical period at the end of the twenty-first century. Saddique et al. [13] explored the impact of climate change on the hydrological regimes of the JRB using the Soil and Water Assessment Tool (SWAT) and reported an increase in annual streamflow. Munawar et al. [14] studied the impact of climate change on streamflow in the JRB by utilizing the Statistical Downscaling Method (SDSM) method for RCP scenarios and found a 3.3–7.4% increase in discharge for 2100 relative to the baseline period. Azmat et al. [15] employed the Hydrological Modelling System (HEC-HMS) and the Snowmelt Runoff Model (SRM) to examine future climate and cryosphere impacts on the hydrology of the JRB and they reported that the average annual streamflows of the catchment are expected to increase by 28%, for RCP8.5 using HEC-HMS and by 26.3% for RCP8.5 using SRM, during 2090s. On the other hand, studies also reported a decrease in the future discharge for the JRB. For instance, Ahsan et al. [16] employed a SWAT model and reported a decrease in future discharge by 23–37% for RCP4.5 and 19–46% for RCP8.5. Another study by Rizwan et al. [17] employed the Integrated Flood Analysis System (IFAS) model and found a decrease of – 37% to – 43% in the annual average flow for the ensemble of General Circulation Models (GCMs) in the JRB. In light of future projections, climate change will significantly alter the hydrological regime of the JRB, requiring the implementation of adaptive water resource management practices.

The previous studies have problems regarding the consistency of the forcing datasets for impact assessment. For instance, different bias-correction and downscaling techniques were used and the climate-forcing datasets used were not trend-preserving. Such shortcomings of the datasets induce inconsistency and ultimately influence future projections. Against this backdrop, there is a need for a consistent approach to overcome these problems. Therefore, standardized, bias-adjusted climate-forcing datasets prepared under the protocol of the Inter-Sectoral Impact Model Intercomparison Project (ISIMIP) were utilized to conduct impact analysis. The ISIMIP offers a GCMs driven historical and future climate under ISIMIP3b employing a variety of GCMs and different emission scenarios, ranging from optimistic to business as usual.

Projections of climate change have been extensively studied using GCMs [18]. The GCM mathematically depicts the general circulation of a planet's atmosphere or ocean [4]. The development of each GCM is based on its own set of assumptions and mathematical representations of the physical processes that shape the climate system, leading to a range of climate projections [19]. These models simulate changes in the climate based on potential future rates of greenhouse gas emissions. GCMs provide large-scale forecasts for several climatic variables, but their coarser

resolution makes it difficult to accurately determine climatic variables. Similarly, these GCM outputs cannot resolve fine-scale basin processes because of their coarse resolution [20, 21]. It is generally advised to use an ensemble technique of different GCMs rather than a single GCM to envisage the future climate because this strategy could manifest diverse scenarios [5, 22]. Different downscaling methods are frequently used to downscale projected GCM data to a fine resolution to solve this problem, but these methods also introduce systematic deviations. Downscaling methods, such as Dynamical and Statistical techniques, are required to use GCM outputs at the basin scale. The dynamical downscaling method utilizes a fine-resolution and computationally intensive Regional Climate Model (RCM) that incorporates coarse-resolution GCM outputs to generate fine-resolution data useful for analyzing basin-scale dynamics. In contrast, statistical downscaling techniques create computationally efficient statistical relationships between the observed fine-scale variables and coarse GCM scale variables to estimate fine-scale future climate.

To outline the future vulnerability thresholds for society and ecosystems, impact models that can accurately interpret climate change signals are relevant for making efficient decisions. Impact models provide information that aids decision-makers and policymakers in creating long-term adaptation plans that are apposite to uncertain future conditions [23]. Therefore, the Soil and Water Integrated Model (SWIM) was employed in this research to unfold the discharge dynamics of the JRB under various climate change scenarios. To the best of our knowledge, no research has been conducted to determine how climate change may affect water resources in the JRB using the SWIM. This study is of great significance due to the highly dynamic and shifting climate of the Jhelum River Basin, where water resources are increasingly threatened by climate change. Even small changes in the region's hydroclimatology could have severe consequences, as the Jhelum River and its tributaries depend heavily on the seasonal temperature and precipitation fluctuations for their streamflow. Additionally, with the help of this study, concerned authorities may be able to manage better and allocate precious water resources by making their management strategies more efficient in mitigating the future impacts of climate change.

2 Study area

Jhelum River is the major tributary of the main Indus River. Its catchment area is located between 73 and 75.62 ºE and 33–35 ºN (Fig. 1). Most of the basin area is on a moderate to steep slope. The mountains in the north are permanently covered with snow [13, 24]. The elevation ranges from 232 to 6285 m above sea level [25]. The basin hosts a wide variety of vegetation species, including subtropical conifer forests, alpine meadows, grassland, and agricultural fields. It contains two major soil groups: cambisols and leptosols [12]. Leptosols are very narrow soils over a hard rock or deeper soil that is extremely gravelly, whereas cambisols are young with barely any noticeable soil formation. The details of the land cover and soil types are shown in Figure S1 and Tables (S1-S2) of the supplementary material.

The basin's average annual maximum temperature is 30.8 °C, while the average annual minimum temperature is 0.3 °C [13]. The station with the lowest average air temperature in the basin is Naran, where the wintertime low is below 0 °C and the summertime high is only 16 °C [13]. The two seasonal precipitation regimes that dominate the basin's precipitation dynamics are the monsoons in the summer and western disturbances in the winter [26]. Between 1961 and 2012, the basin's mean annual precipitation was 1196 mm [27]. The winter season accounts for nearly 38% of the mean annual rainfall, with the summer season accounting for the remaining 62% [15]. Approximately 65% of the basin's surface is covered in snow during the winter and only 3% of it is by the end of summer [15] whereas about 1% of the basin is covered by glaciers [28].

The Jhelum River is contributed by three major tributaries Kunhar, Neelum, and Poonch. The Great Himalayas' southern slope and the Pir Punjal Mountains' northern slopes are drained by the Jhelum River and its main tributaries, the Kunhar and Neelum. Another important tributary, the Kanshi River directly joins the Jhelum River at Mangla Lake. According to the observations made between 1976 and 2005, the annual mean runoff of JRB at Azad Pattan is 833 m^3s^{-1}. In June, Azad Pattan experienced its 1741 m^3s^{-1} maximum discharge, while the minimum discharge of 223 m^3s^{-1} occurred in January [13]. The JRB receives significant runoff contributions from snowmelt but negligible from glacier melt during spring and early summer (April to mid-June), while monsoon precipitation makes a significant contribution during summer and early autumn (end of June to September). The basin ultimately drains into the country's second-largest Mangla reservoir, constructed in 1967 with a gross capacity of 7.29 km^3 [15]. The reservoir receives more than 75% of its total water supplies during the high flow period of March to August [29]. The Mangla Reservoir irrigates six million hectares of agricultural land [30] and contributes 6% of the nation's hydropower production.

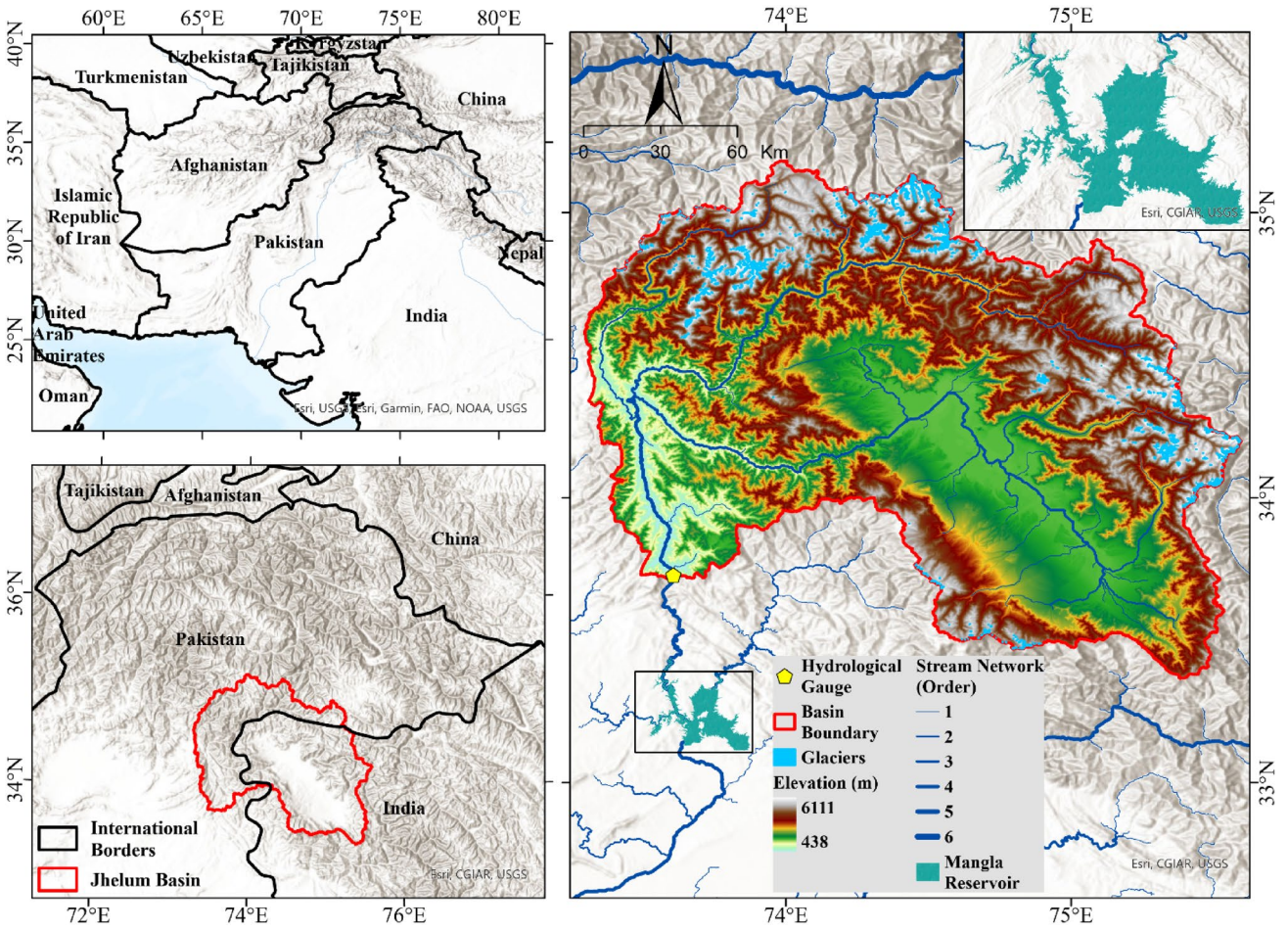

Fig. 1 Study area of the transboundary Jhelum River Basin, western Himalaya

3 Materials and methods

3.1 Datasets

3.1.1 Hydro-climatic data

The climate input datasets from the ISIMIP framework were obtained, which under its 3b protocol provides the bias-adjusted CMIP6 experiments for the historical period and for three future scenarios of SSP1-2.6 (SSP1-RCP2.6), SSP3-7.0 (SSP3-RCP7), and SSP5-8.5 (SSP5-RCP8.5) at 0.5° spatial and daily temporal resolutions. These datasets are prepared by adjusting biases and statistically downscaling experiments from five CMIP6 ESMs (GFDL-ESM4, IPSL-CM6A-LR, MPI-ESM1-2-HR, MRI-ESM2-0, and UKESM1-0-LL) against the W5E5v2.0 observational dataset using ISIMIP3BASD v2.5.0 algorithm [31–34]. To calibrate and validate the SWIM model, the observed Jhelum river discharges at the Azad Patan gauge were obtained from the Surface Water Hydrology Project (SWHP) of the Water and Power Development Authority (WAPDA), Pakistan for the 1994–2004 period. Table 1 shows the summary of the hydro-climatic datasets that were employed in this study.

3.1.2 Geospatial data

To define the Jhelum watershed up to the Azad Pattan gauging site, analyze its topographical features, and examine drainage patterns, the Shuttle Radar Topography Mission (SRTM) Digital Elevation Model (DEM) (https://earthexplo

Table 1 Summary of the hydro-climatic datasets

Dataset	Data Source	Data Type	Resolution	Time Span	
				Historical	Future
GFDL-ESM4	ISIMIP3b	Simulated Climate	0.5° Daily	1985–2014	2016–2100
IPSL-CM6A-LR	ISIMIP3b	Simulated Climate	0.5° Daily	1985–2014	2016–2100
MPI-ESM1-2-HR	ISIMIP3b	Simulated Climate	0.5° Daily	1985–2014	2016–2100
MRI-ESM2-0	ISIMIP3b	Simulated Climate	0.5° Daily	1985–2014	2016–2100
UKESM1-0-LL	ISIMIP3b	Simulated Climate	0.5° Daily	1985–2014	2016–2100
W5E5v2.0	ISIMIP	Observed Climate	0.5° Daily	1994–2004	
Jhelum at Azad Pattan	WAPDA	Observed Discharge	Daily	1994–2004	

rer.usgs.gov/) was obtained from the United States Geological Survey [35]. The soil distribution was obtained from the United Nations Harmonized World Soil Database (HWSD) of the Food and Agriculture Organization (FAO). The HWSD is a raster dataset with 30 arc seconds that contains more than 15,000 unique soil mapping units [36]. The land use and land cover features were extracted from the GlobCover global land cover map for 2009, prepared at a 300-m planar resolution based on imagery from the MERIS sensor on board the ENVISAT satellite [37]. The GlobCover land use classification was translated to 15 land cover classes used by the SWIM. Glacier ice thickness data was taken from the Randolph Glacier Inventory version 6.0 [38] prepared by Farinotti et al. [39].

3.1.3 Shared socioeconomic pathways

The SSPs manifest five distinct global states (SSP1–5) with noticeably different socioeconomic circumstances [40, 41]. Following the ISIMIP3b protocol, the study analyzes projections of the Jhelum streamflow only under SSP1-2.6, SSP3-7.0, and SSP5-8.5. The SSP1 is a sustainability scenario that depicts a sustainable world where mitigating and adapting to climate change is manageable due to low-income countries' swift economic growth, reduced disparity, fast technological signs of progress, and extensive consciousness of ecological degradation. Additionally, included in the scenario are effective technologies for agricultural land that increase yield. The SSP3, a fragmentation scenario, characterizes situations where it is cumbersome to mitigate and adapt to climate change due to extreme poverty and a quickly expanding population. The environment is seriously demeaning, and technological advancement in the energy sector is lethargic. The utilization of local energy resources is improved by the limited synchronization between regions. The SSP5 corresponds to conventional development, in which adaptation is made simple by robust economic growth, but mitigating climate change impacts would be challenging due to the supremacy of fossil fuels in the energy system. The agroecosystems will be well-managed and benefit from the agricultural industry's rapid technological development. According to the RCP scenarios, RCP2.6 is an optimistic pathway in which CO_2 emissions start to decline by 2020 and reach zero by 2100. RCP8.5 is considered a worst-case scenario where emissions continue to increase throughout the twenty-first century. The SSP1-2.6 scenario, an update of RCP version (2.6 Wm^{-2}), is associated with the Paris Agreement, which aims to limit global warming to 2.0 °C by 2100. The SSP3-7.0 is a newly introduced scenario to narrow down the gap between RCP6.0 and RCP8.5 and in this scenario, the total radiative forcing is predicted to increase to roughly 7.0 Wm^{-2} [42]. In SSP5–8.5, the levels of radiative forcing are predicted to increase to roughly 8.5 Wm^{-2} by the year 2100.

3.2 Methodology

The methodological framework of the study is shown in Fig. 2. The eco-hydrological model SWIM was set up for the JRB up to the Azad Pattan discharge gauging site. The model has been validated for the hydrological years of October 1994 to September 1999 after being calibrated for the hydrological years of October 1999 to September 2004. The validated model was run for the historical (1985–2014) and future (2016–2100) climates. The future climate inputs provided by the ISIMIP-3b are derived from five ESMs for three SSP scenarios (SSP1-2.6, SSP3-7.0, and SSP5-8.5). For each scenario and ESM, the temperature, precipitation, and streamflow changes were evaluated for the near-future (2016–2043), mid-future (2044–2071), and far-future (2072–2100) climates relative to the historical climate.

A nonparametric Mann–Kendall (MK) test was applied to identify trends [43, 44] and utilized the Theil-Sen method to estimate the trend slope [45, 46]. These approaches do not necessitate normal distribution of time series data [47] and are robust against missing values, outliers, and discontinuities [48]. The MK test is commonly employed for

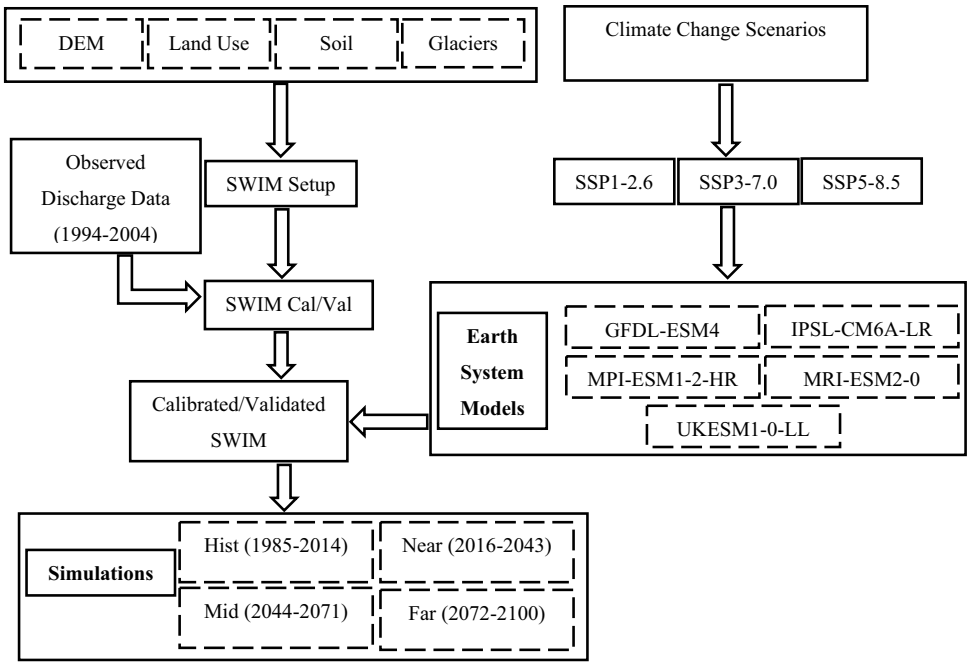

Fig. 2 Methodological framework of the present study

detecting monotonic trends in hydrometeorological time series, as extensively discussed in various studies [49, 50]. To mitigate the impact of serial dependence in naturally observed time series, a modified version of the MK test was utilized. This modification involves pre-whitening the time series for autoregressive processes before assessing a trend [49, 51].

3.2.1 Hydrological modelling

The SWIM offers a GIS-based tool for the coupled modeling of hydrology, vegetation, and water quality that can be parameterized using locally accessible data. The model can thus be employed to analyze how changes in land use and climate impact regionally scaled changes in water quality, agricultural yield, and hydrological processes [99]. The water balance equation forms the basis of the hydrological module, which incorporates precipitation, evapotranspiration, percolation, surface runoff, and subsurface runoff for the soil profile spanning over several layers. The SWIM employs a three-level disaggregation scheme like MATSALU [100], which assumes basins, sub-basins, and hydrotopes inside of sub-basins. A basin is first divided into sub-basins with sizeable areas, and further into hydrotopes or Hydrologic Response Units (HRUs), which are defined by particular soil type and land use and are assumed to behave hydrologically uniformly throughout the sub-basin. As meteorological input data, the SWIM uses daily precipitation, average, minimum, and maximum temperatures, solar radiation, and relative humidity.

3.2.2 Model performance metrics

The Percent Bias (PBIAS), Nash–Sutcliffe Efficiency (NSE), coefficient of determination (R^2), Root Mean Squared Error (RMSE), Volumetric Efficiency (VE), and Mean Error were used to evaluate the SWIM performance against observed discharges. The value of R^2 ranges from zero to one, with one indicating a perfect fit and zero indicating a poor fit. The NSE ranges from minus infinity to one quantifies how closely the observed discharges match the simulated discharges. Percent Bias has an ideal value of zero, whereas low PBIAS manifests good model simulation. Positive values of PBIAS indicate model underestimation, whereas negative values suggest model overestimation. Lower values of RMSE indicate good model fit. The value of VE ranges between zero and one. For the daily simulated flows, Moriasi et al. [52] considered the performance of the watershed-scale model to be "satisfactory" if the conditions of $R^2 > 0.60$, NSE > 0.50, and PBIAS < ± 15% are satisfied. As shown in Table 2, four performance evaluation classes based on R^2, NSE, and PBIAS were considered.

Table 2 Summary of the flow performance evaluation criteria for the daily temporal scale, Moriasi et al. [52]

	Performance Evaluation Criteria			
Measure	Very Good	Good	Satisfactory	Unsatisfactory
R^2	$R^2 > 0.85$	$0.75 < R^2 \leq 0.85$	$0.60 < R^2 \leq 0.75$	$R^2 \leq 0.60$
NSE	NSE > 0.80	0.70 < NSE ≤ 0.80	0.50 < NSE ≤ 0.70	NSE ≤ 0.50
PBIAS	PBIAS < ± 5	± 5 ≤ PBIAS < ± 10	± 10 ≤ PBIAS < ± 15	PBIAS ≥ ± 15

R^2 refers to the coefficient of determination, NSE refers to Nash–Sutcliffe Efficiency, and PBIAS is the Percentage Bias

3.2.3 Mean changes

First, the focus was on the variation of the mean annual and seasonal changes in temperature, precipitation, and flows for the historical and future periods. Seasonal scale changes in streamflow were analyzed according to the seasons defined as MS: Monsoon (JAS), SA: Snow Accumulation (ONDJF), and SM: Snow Melt (MAMJ). Furthermore, the distribution of the aforementioned variables in terms of the annual cycle was studied. The emergence of temperature, precipitation, and flows relative to the baseline period was also analyzed. Moreover, the Gini coefficient (GC) was computed to investigate the distribution of annual flows. The MK test was applied to study the trends of historical and future mean annual temperature and discharge along with the total annual precipitation. Moreover, the MK test was also applied to assess the variation of historical and future flows in terms of GC.

3.2.3.1 Emergence of temperature, precipitation, and discharge Anthropogenic influences are leading to a warming Earth, altering the temperature, precipitation, and discharge patterns. These changes become most relevant when a new climate emerges, differing significantly from an undisturbed or a given baseline state. Determining when changes emerge is crucial for informing the development of adaptation and mitigation strategies [53, 54]. Past efforts to determine the emergence have primarily focused on mean temperature and precipitation [55–58]. Nevertheless, few studies have also focused on the emergence of river discharges. John et al. [59] analyzed the time of emergence of climate-induced variations in river discharge across Australia. Muelchi et al. [60] analyzed variation in runoff regimes and their time of emergence for 93 catchments in Switzerland. Here we investigate the emergence to determine the year when change signals in hydroclimatic timeseries become detectable. The change signal is considered to have emerged when it departs beyond the mean plus (or minus) standard deviation of the baseline period on a 31-year running mean timeseries within the 1985–2100 period.

3.2.3.2 Gini Coefficient The GC is a widely used measure for quantifying distribution. It was originally employed to assess income inequality among households in economics and has been used in ecological and biological studies to evaluate inequality in the size distribution among individuals. Jawitz and Mitchell [61] utilized the GC to analyze hydrological inequality. The GC was computed to quantitatively assess future changes in annual streamflow inequality following:

$$G = 1 + \frac{1}{n} - \frac{2\sum_k r_k x_k}{n\sum_k x_k}$$

Here, x_k represents the value, and r_k denotes its rank in descending order. The highest value x_k is assigned a rank of r_k =1, the second-highest as r_k=2, and so forth. When applied to daily streamflow, a GC value of one indicates that a single day contributed to the yearly streamflow, while a value of zero signifies a uniform distribution. In this study, the GC is computed for yearly daily streamflow values, covering the period 1985–2100.

3.2.4 Extreme changes

Secondly, to investigate the extremes, the Gumbel distribution was used in this study to analyze changes in flood levels induced by climate change [62, 63]. The annual maximum discharges were fitted using the Gumbel distribution, and changes in the 30-year flood levels were estimated. The location parameter and the scale parameter serve as the two defining characteristics of the Gumbel distribution. By using a block-maximum strategy, the peak

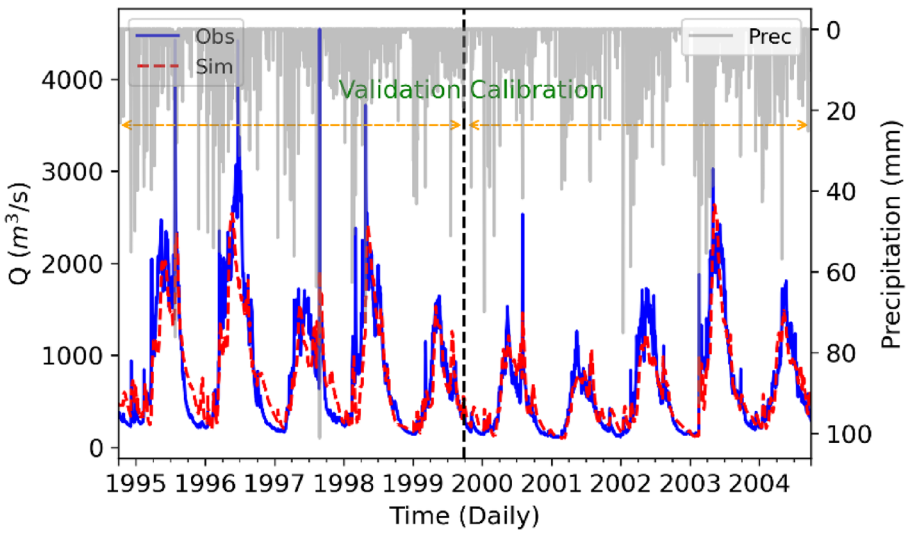

Fig. 3 Comparison of daily observed and simulated discharges for the calibration (1999–2004), validation (1994–1999), and overall (1994–2004) periods

Table 3 SWIM calibration and validation statistics

Basin	Procedure	Period (Oct-Sep)	NSE	PBIAS	VE	ME	R^2	RMSE (m^3s^{-1})	Overall (Moriasi et al.52)
Jhelum	Calibration	1999–2004	0.83	– 0.50	0.76	– 3.02	0.84	206.08	Very Good
	Validation	1994–1999	0.73	– 5.40	0.71	– 47.97	0.75	379.24	Good
	Overall	1994–2004	0.78	– 3.30	0.73	– 24.75	0.78	305.12	Good

NSE (Nash–Sutcliffe Efficiency), *PBIAS* (Percent Bias), *VE* (Volumetric Efficiency), *ME* (Mean Error), R^2 (Coefficient of Determination), *RMSE* (Root Mean Square Error)

flow event for each year was chosen. Gumbel's probability distribution is frequently used in extreme value theory for analyses of flood frequency to assess the impact of climate change on floods [64, 65]. Moreover, the changes in low, medium, and high flows in terms of 10th, 25th, 50th, 75th, and 90th percentiles (P10, P25, P50, P75, and P90) were quantified. The MK test was applied to analyze the trends of low, medium, and high flows.

4 Results

4.1 SWIM calibration and validation

The observed and simulated daily streamflow along with observed precipitation (W5E5v2.0) during the calibration and validation period is shown in Fig. 3. The sensitive SWIM parameters were tuned to produce the best possible agreement between the simulated and observed discharge. The model parameters finalized during the calibration period were used to simulate the discharge during the validation period. The results of the model evaluation criteria are shown in Table 3. The values of NSE and R^2 during the calibration were 0.83 and 0.84 respectively while during the validation period, NSE and R^2 were 0.73 and 0.75 respectively. The underestimation of the high flows and overestimation of the low flows was also observed during the calibration and validation periods. The validation period manifests high peaks owing to the heavy precipitation while during the calibration period, a prolonged dry spell was observed with relatively low peaks. According to the model performance criteria defined by Moriasi et al. [52], the overall outcome of the model simulation was classified as good. Hence, it indicates that SWIM can efficiently generate the simulated discharge with reasonable accuracy.

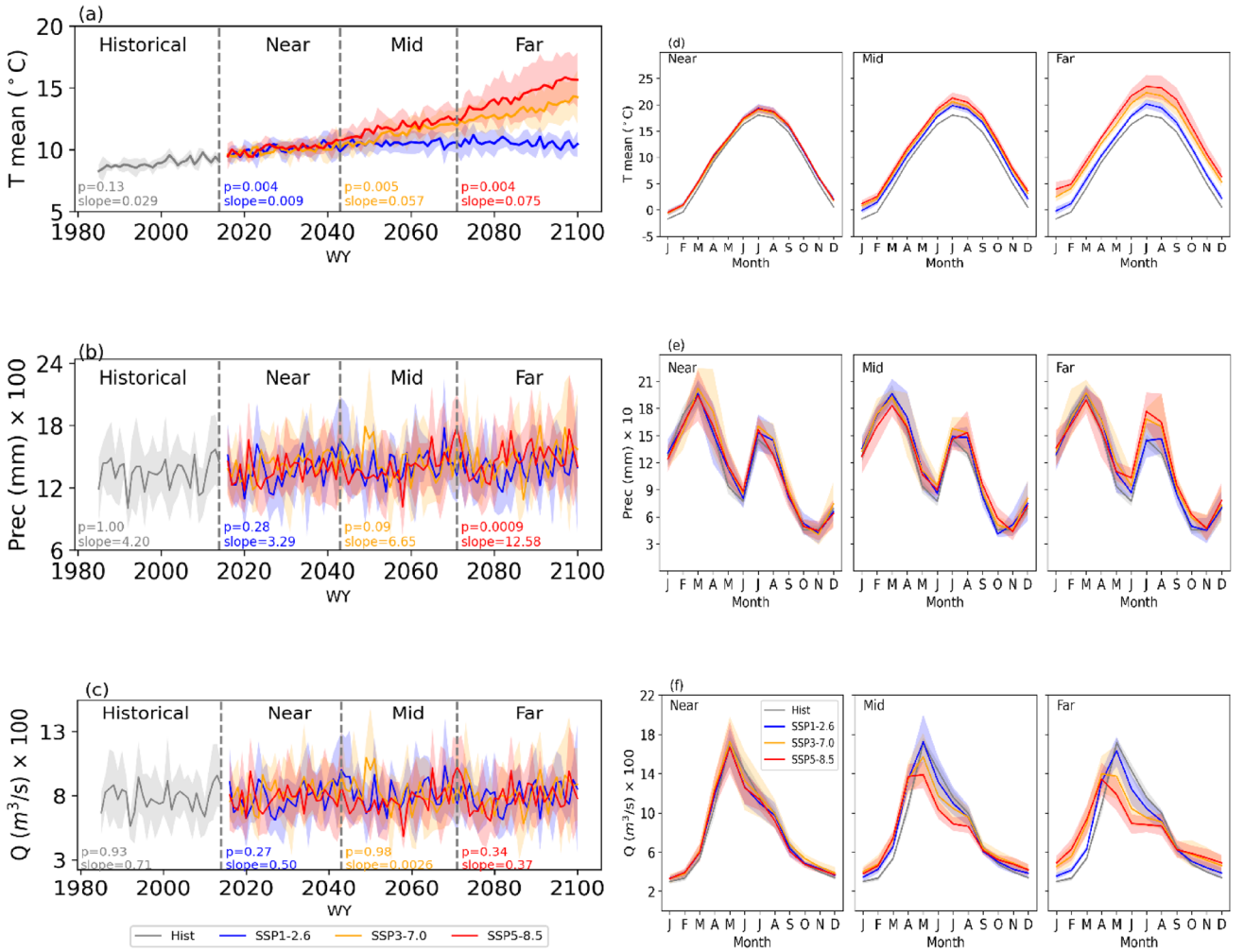

Fig. 4 Annual Historical and future **(a)** mean temperature and **(b)** total precipitation and **(c)** mean discharge trends under SSP1-2.6, SSP3-7.0, and SSP5-8.5 in the JRB. Long-term variation of **(d)** temperature **(e)** precipitation and **(f)** discharge under SSP1-2.6, SSP3-7.0, and SSP5-8.5 during the three future climates relative to the historical period. Note: The shaded background region indicates the model spread (Standard Deviation)

4.2 Mean changes

4.2.1 Future temperature, precipitation, and discharge projections

The projected increase in mean temperature is more pronounced under the high-end warming scenarios of SSP3-7.0 (0.057 °C/year) and SSP5-8.5 (0.075 °C/year), Fig. 4a. For all three future climates under SSP1-2.6, SSP3-7.0, and SSP5-8.5 scenarios, the monthly mean temperatures were projected to be higher than the historical period (1985–2014) shown in Fig. 4d. The projected increase in the mean temperature is in line with the study conducted by Munawar et al. [14] where they reported an increase of 1.5 to 3.8 °C relative to the reference period. Overall, the temperature increase is projected to be more pronounced for the high-end warming scenario of SSP5-8.5. The ensemble Tmean was projected to increase between 1.01 and 5.46 °C as shown in Table 4. Following the three SSP scenarios, Fig. 5a manifests the ensemble mean (intermodel mean of five ESMs) change in the monthly mean temperatures for the three future periods relative to the historical period. In September compared to the other months, the variation in Tmean was higher specifically for the high-end warming scenarios.

Figure 4b shows the ESMs precipitation projections for the three future periods under the three SSP scenarios. In all scenarios, a rising trend was observed. Under SSP5-8.5, the increment was higher than it was under SSP3-7.0 and

Discover Applied Sciences (2025) 7:308 | https://doi.org/10.1007/s42452-025-06721-y

Table 4 Variation of Tmean (°C), Precipitation (%), and Discharge (%) under SSP1-2.6, SSP3-7.0, and SSP5-8.5 scenarios during the three future climates (near, mid, and far), relative to the historical period (1985–2014)

Scenario	Change in Tmean (°C)						Change in Precipitation (%)						Change in Discharge (%)					
	GFDL	IPSL	MPI	MRI	UKESM	Ens	GFDL	IPSL	MPI	MRI	UKESM	Ens	GFDL	IPSL	MPI	MRI	UKESM	Ens
SSP1-2.6																		
Near	0.62	1.29	0.63	1.23	1.70	1.09	1.11	1.94	6.27	0.79	0.15	2.08	− 1.16	− 0.57	5.85	− 0.92	− 2.99	0.09
Mid	1.24	1.73	0.86	1.78	2.40	1.60	− 2.28	5.61	***13.58***	3.69	5.88	5.34	− 7.30	0.65	***19.11***	1.04	2.26	3.84
Far	1.09	1.67	0.93	1.73	2.73	1.63	3.19	4.04	6.13	0.88	3.74	3.61	1.24	0.15	6.58	− 2.40	-0.47	1.08
SSP3-7.0																		
Near	0.57	1.24	0.49	1.13	1.61	1.01	− 3.95	5.65	***17.19***	3.89	4.09	5.44	− 7.55	4.96	***20.58***	2.48	1.94	4.61
Mid	1.81	2.86	1.54	2.37	3.35	2.39	− 2.23	2.64	***13.53***	6.01	***15.17***	7.05	− 6.79	− 4.16	***14.07***	2.85	***13.80***	4.07
Far	3.43	***5.41***	2.81	3.68	***5.60***	4.18	− 5.62	1.92	***17.16***	9.17	***26.02***	9.74	− ***14.07***	− 8.74	***15.89***	3.55	***20.79***	3.63
SSP5-8.5																		
Near	0.98	1.17	0.82	1.33	1.71	1.20	− 6.22	1.41	5.87	4.18	4.15	1.89	− ***12.06***	− 2.21	5.63	4.17	2.44	− 0.16
Mid	2.11	3.29	1.97	3.17	4.05	2.92	− 5.53	3.60	6.09	2.21	***11.85***	3.64	− ***13.22***	− 5.20	3.65	− 3.86	5.16	− 2.64
Far	4.07	***7.57***	3.89	4.80	***6.96***	***5.46***	− 4.60	7.11	***17.81***	8.23	***21.47***	***10.03***	− ***16.36***	− 7.39	***11.78***	0.25	***13.34***	0.44

Change of more than 5 °C and ± 10% is shown in bold italic

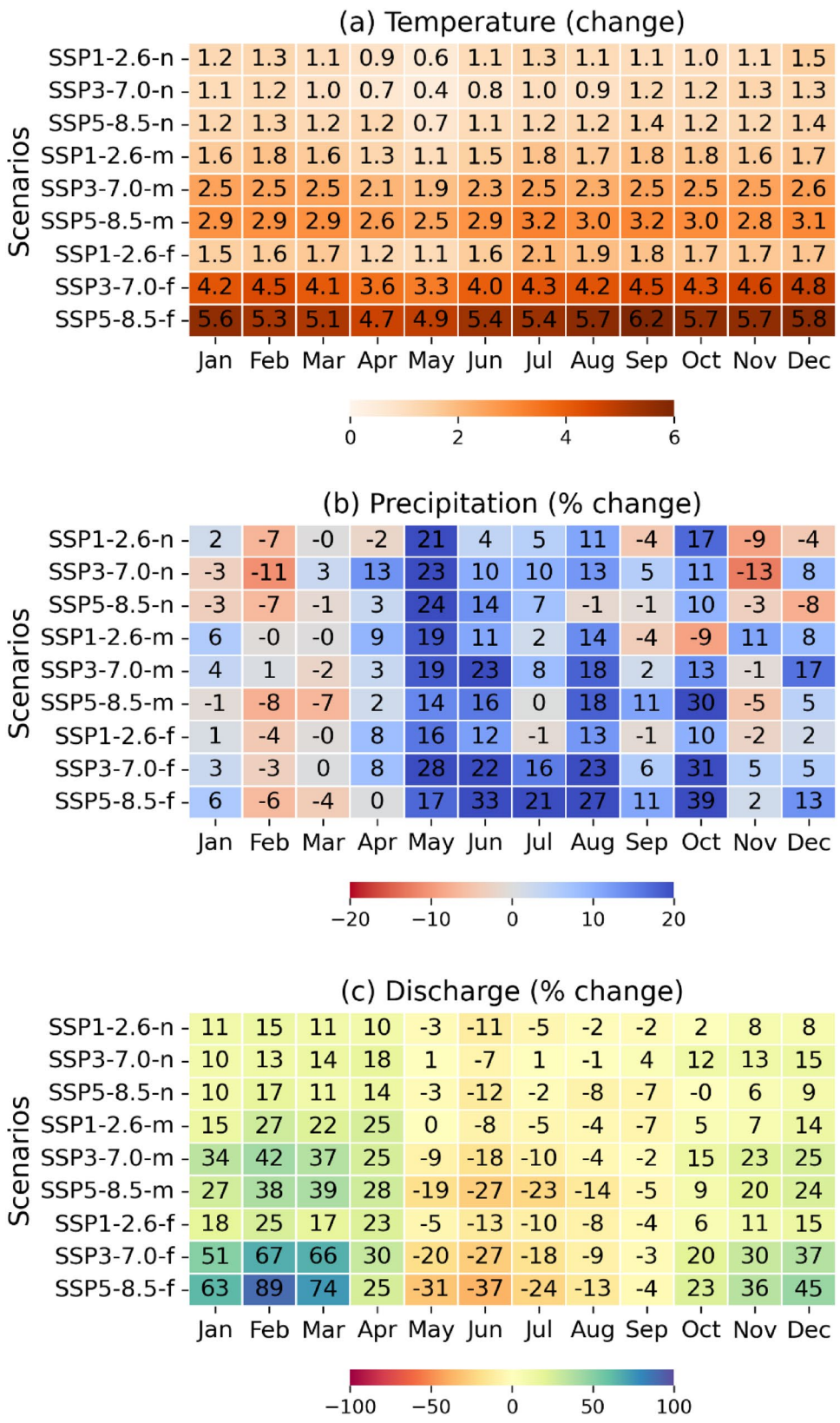

Fig. 5 Long-term monthly change in (**a**) Tmean (°C) (**b**) precipitation (%) and **(c)** discharge (%) relative to the historical period (1985–2014)

SSP1-2.6. With a p-value less than 0.05 at the 95% confidence interval, the modified Mann–Kendall test revealed a significant rising trend in precipitation for the SSP5-8.5 scenario. With the Thiel-Sen slope estimator, SSP5-8.5 showed an increasing slope of 12.58 mm/year. According to the SSP1-2.6, SSP3-7.0, and SSP5-8.5 scenarios, Table 4 shows the projected change in precipitation for the three future climates relative to the historical period. According to the GFDL model, the precipitation is projected to decrease under high-end warming scenarios of SSP3-7.0 and SSP5-8.5 for all three future climates, ranging between −2.23 to −5.62% under SSP3-7.0 and − 4.60 to − 6.22% under SSP5-8.5. The ensemble mean data projected that precipitation would rise throughout the study period from 2.08 to 5.34% under SSP1-2.6, 5.44 to 9.74% under SSP3-7.0, and 1.89 to 10.03% under SSP5-8.5. The highest variation in future precipitation relative to the historical period was projected by UKESM out of the five ESMs, specifically 26.02% and 21.47% for the high-end warming scenarios of SSP3-7.0 and SSP5-8.5 respectively. The variation of long-term monthly precipitation relative to the historical period is shown in Fig. 4e. Two distinct precipitation peaks were observed during March and July [70]. The summer monsoon (June–July–August–September), which results from southwestern winds from the Bay of Bengal and the Arabian Sea, causes the peak in July while the Western Disturbances (WDs) system in the winter is responsible for the other peak in March. Furthermore, the annual cycles of rain (liquid precipitation) and snow (solid precipitation) for the historical and future periods are shown in the supplementary material (Figure S2). Figure 5b manifests the ensemble mean change in the monthly precipitation for the three future periods under three different SSP scenarios. Precipitation was projected to decrease in February (−8 to −6%) and March (−7 to −1%) while increasing in May (14 to 24%), June (14 to 33%), July (7 to 21%), and October (10 to 39%) for all future climates under the high-end warming scenario of SSP5-8.5. In August and September, precipitation was also projected to increase except for a slight decrease of −1% in the near future under the SSP5-8.5 scenario.

Figure 4c shows the ESM annual mean discharge variations for the historical and three future periods under the three SSP scenarios. No significant rising or falling trend was observed for the annual mean future discharge projections under all climate change scenarios. However, we found significant rising and falling trends in the yearly mean discharge of snow accumulation and monsoon season respectively, under the high-end warming scenarios of SSP3-7.0 and SSP5-8.5 (Figure S3). The annual cycles of historical (1985–2014), and projected (2016–2100) discharges for three 21st-century climates under three different SSP scenarios are shown in Fig. 4f. All SSPs project a peak discharge during May and this peak shift towards April for the far-future climate under the high-end warming scenarios of SSP3-7.0 and SSP5-8.5. This shift in peak discharge is primarily attributable to the earlier snowmelt [15, 72]. All the models under consideration show no change in the timing of the peak discharge under the SSP1, SSP3, and SSP5 scenarios for the near-future climate. The catchments at high elevations are particularly vulnerable to changes in the timing of runoff generation [73]. Overall, a decrease in the magnitude of the peak discharge is observed for all the future climates relative to the historical period, where such a decrease is more pronounced for the high-end warming scenarios.

An overall decrease in the discharge is observed for all the future climates under the high-end warming scenario (SSP5-8.5) except for the discharge obtained via MPI-ESM and UKESM. Also, the near and far future climates of MRI under SSP5-8.5 show an increase in the discharge. Specifically, for the Intermodel ensemble mean, the discharge will reduce by −0.16% and −2.64% in the near and mid-future respectively, under SSP5, Table 4. The near, mid, and far future climates of MPI-ESM show an increase in discharge for all three SSP scenarios, notably, 20.58% in the near future and 15.89% in the far future under SSP3-7.0. Likewise, 19.11% in the mid-future under SSP1-2.6. The UKESM projects a rise in the discharge by 2.44, 5.16, and 13.34% in the near, mid, and far future respectively, under SSP5-8.5.

The comparison between the projected discharge for each month of the future period relative to the historical periods under SSP1-2.6, SSP3-7.0, and SSP5-8.5 is shown in Fig. 5c. It is worth noting that the projected discharge continues to increase during the 7 months, specifically, from January to April and October to December under all the SSP scenarios. Contrarily, under all the SSP scenarios, the projected stream flow mostly decreases during the remaining 5 months, explicitly, from May to September. Hence, the flows during the wet (summer) and dry (winter) periods are projected to decrease and increase respectively relative to the historical period. The likelihood of increased streamflow in the winter and spring is associated with increased winter temperatures [75]. The decrease in future discharge relative to the historical period despite the increase in precipitation during monsoon is mainly attributed to the increase in evapotranspiration. During monsoon, the rate of increase in potential evapotranspiration is higher than the rate of increase in precipitation, implying a decline in future water availability (Figure S4). Secondly, due to the temperature rise, there is a phase change in precipitation (from snow to rain) during the winter months [76]. This shift from solid to more liquid precipitation leads to less snow accumulation in the future relative to the historical period. More rain (liquid precipitation) during winter leads to an increase in future winter discharge relative to the historical period. The percentage change in future snow and rain relative to the historical period under climate change scenarios for the snow accumulation season (ONDJF) is shown

in the supplementary material (Figure S5). The reduction in future snow accumulation and earlier snowmelt due to the rise in temperature leads to decreased water availability in monsoon months [77]. Owing to the less snow accumulation during winter the snowpacks are diminishing therefore a significant decrease in the annual mean snow area and depth was observed for the historical and three future periods under all SSP scenarios (Figure S6).

During the winter and summer months, February shows the maximum increase and June shows the maximum decrease in the discharge respectively under all SSP scenarios. Specifically, 89% increase during February and a 37% decrease during June for the far-future climate under the SSP5-8.5 scenario. In Fig. 5c, it is evident that most of the percentage changes in the mean monthly projected discharge are more pronounced under SSP5-8.5 relative to the low-end

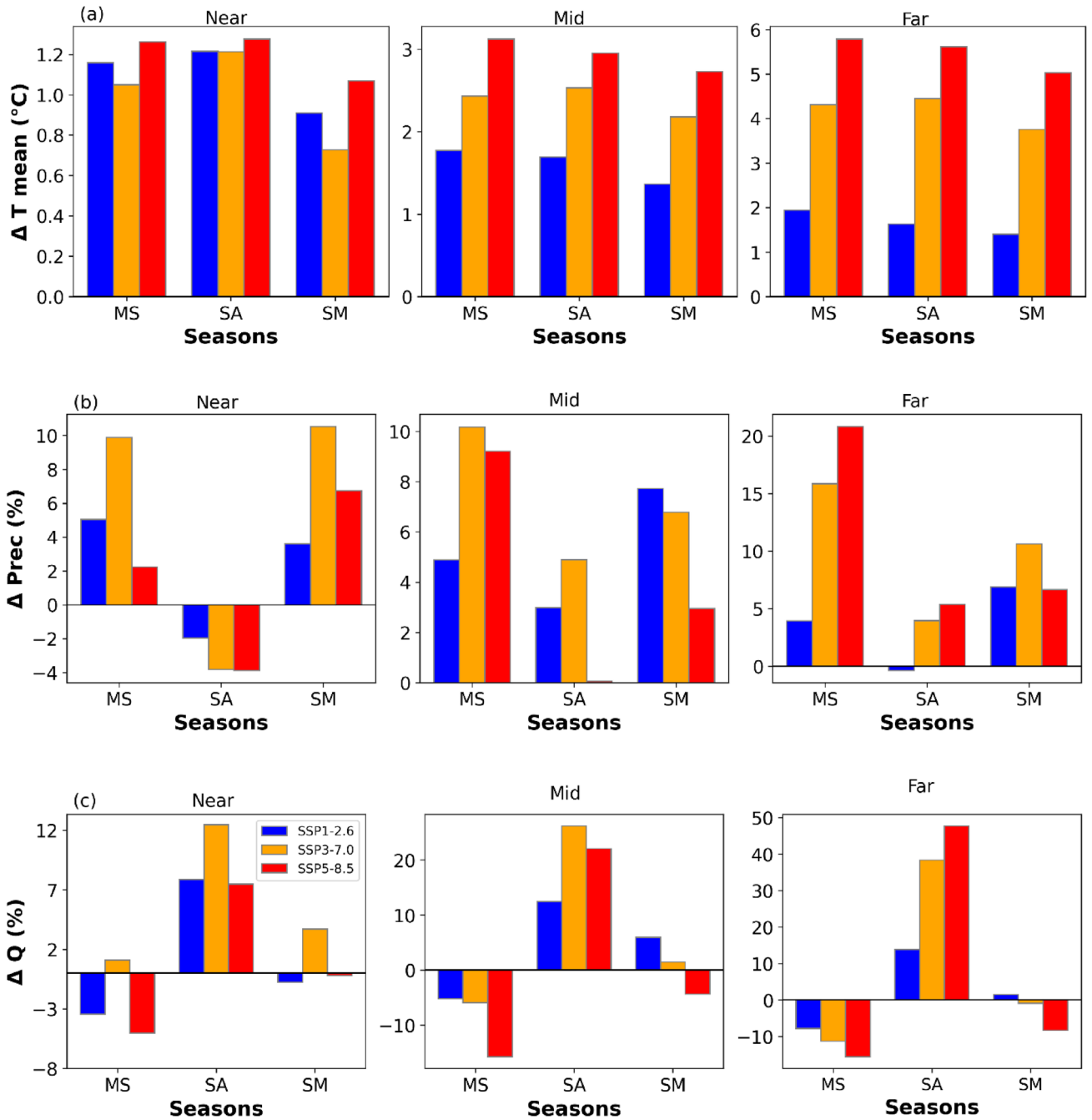

Fig. 6 Seasonal changes in the Jhelum River Basin's **(a)** Mean temperature, **(b)** Precipitation, and **(c)** Mean discharge for future climates under SSP1-2.6, SSP3-7.0, and SSP5-8.5. Note: Seasons are defined as (SA: Snow Accumulation; SM: Snow Melt; MS: Monsoon)

warming scenarios of SSP1-2.6 and SSP3-7.0. The far future period under SSP3-7.0 and SSP5-8.5 manifests more significant flow alterations relative to the near and mid-future climates.

Seasonal variations of temperature, precipitation, and discharge relative to the historical period are shown in Fig. 6. The seasonal analysis revealed that mean temperature across all seasons notably increased relative to the historical period. This warming trend persists consistently in the near, mid, and far-future projections. Under various climate change scenarios, the observed temperature increase is particularly pronounced, for high-end warming scenarios (SSP3-7.0 and SSP5-8.5). Specifically, temperature increase under the SSP5-8.5 scenario is more pronounced during the MS season followed by SA and SM seasons for the mid and far-future climates. In the near future precipitation will increase during the MS and SM seasons while decreasing during the SA season under all SSP scenarios. The reduced precipitation during the SA season is attributed to the reduction in snowfall. During the mid and far-future climates, precipitation increased during all seasons except during SA for the far-future climate under SSP1-2.6 relative to the historical period. The increase was most noticeable for the far-future climate under high-end warming scenarios. The future discharge dynamics show an increase in flows during the SA season a decrease during the MS season (except for the near future under the SSP3-7.0 scenario) and a mixed pattern of increase and decrease during the SM season. The highest increase and decrease are during SA and MS seasons for the far future climate under the SSP5-8.5 scenario respectively.

Under all SSP scenarios, the simulated flows during the SA period are projected to increase for the majority of future climates, except for the few cases of GFDL (SSP1-2.6 mid-future, SSP3-7.0 near future, and SSP5-8.5 near future) and MRI (SSP1-2.6 mid-future and far-future). Specifically, SA ensemble mean discharge is projected to increase by 7.86–13.83% under SSP1-2.6, 12.47–38.39% under SSP3-7.0, and 7.48–47.75% under SSP5-8.5 throughout the future period. In contrast, the SM flows are projected to decrease for the far-future climates under the SSP5-8.5 scenario, except for the MPI and UKESM. Specifically, the ensemble mean SM flows are anticipated to decrease by – 0.79% for the near future under SSP1-2.6, – 0.94% for the far future under SSP3-7.0, and – 8.30% under SSP5-8.5 for the far-future climate. Under the SSP5-8.5 scenario, variations in MS discharge volumes manifest a decrease. The vicissitudes in the ensemble mean MS flows are projected to vary between – 7.78 to – 3.44% under SSP1-2.6, from – 11.27 to 1.09% under SSP3-7.0, and from – 15.74 to – 5.05% under SSP5-8.5. The summary of the projected changes in seasonal temperature, precipitation, and discharge for individual models are shown in (Tables S3-S5) of the Supplementary Material.

4.2.2 Temperature, precipitation, and discharge emergence

First, the mean and standard deviation of the reference period (1985–2014) was calculated. Subsequently, a 31-year moving average spanning from 1985 to 2100 was computed. Remarkably, by 2025, the temperature (9.31 °C) surpassed the mean plus one standard deviation (9.27 °C) of the reference period as shown in Fig. 7a. This pivotal event signals a notable deviation from the historical temperature patterns, indicating a potential shift in climatic trends. The emergence of mean temperature beyond this threshold in 2025 under the high-end warming scenario of SSP5-8.5 underscores the significance of ongoing climate changes. Such an emergence of temperature could accelerate snowmelt and alter

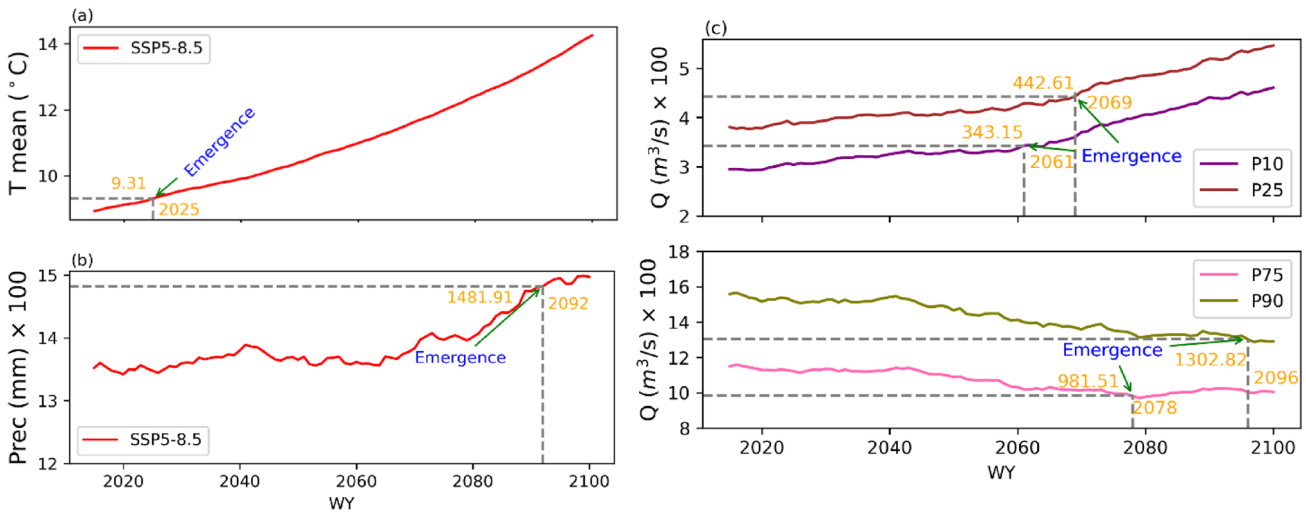

Fig. 7 Future emergence of **(a)** temperature **(b)** precipitation, and **(c)** discharge relative to the historical period under the SSP5-8.5 scenario

precipitation patterns, impacting the timing and volume of streamflow. Secondly, rising temperatures may reduce snowpack accumulation or accelerate melting, affecting the availability of water for downstream flow. Moreover, Increased temperatures can intensify evaporation rates, potentially leading to decreased water availability. Similarly, precipitation emergence was also computed considering the same reference and future periods. We found that the precipitation (1481.91 mm) emerged by 2092 relative to the reference data (1480.68 mm), Fig. 7b. Figure 7c shows the emergence of low (P10 and P25) and high (P75 and P90) flows under the SSP5-8.5 scenario. The low flows are projected to increase relative to the historical period and we found that P10 emerged earlier (2061) than P25 (2069). On the contrary, projections indicate a decrease in high flows compared to the historical period, and our findings reveal that P75 emerged earlier in 2078 than P90, which emerged in 2096. Leng et al. [85] investigated the emergence of hydrological variations in surface water resources across the conterminous United States in response to future warming. A study conducted in the Hanjiang River watershed used climate model ensembles to analyze the timing of climate change emergence from internal variability for hydrological impact studies [86].

4.2.3 Gini coefficient

The GC analysis revealed a decreasing trend for the streamflow under all future scenarios relative to the historical period as shown in Fig. 8. The yearly daily flows during the historical period were more concentrated during the high flow periods and less during the low flow periods which resulted in an unequal distribution of flows. In contrast, during the future periods, a reduction in the high flows during the summer months was observed while an increase in the low flows during the winter months. Such a future pattern of streamflow distribution results in lower values of GC resulting in a comparatively equal distribution of flows. The lower values of GC are more pronounced for the high-end warming scenario of SSP5-8.5. Similarly, Ye et al. [87] applied the Mann–Kendall test and reported a declining trend in GC across six Karst watersheds. The GC, allows us to investigate the pattern of intra-annual variability in river discharge [87]. In a recent study, Kuntla et al. [88] used an observational streamflow dataset and GC to investigate the spatiotemporal variations in streamflow inequality.

4.3 Extreme changes

4.3.1 Flood frequency analysis

Analyses of flood frequency were conducted using the simulated discharge. The projected changes in flood return periods up to 100 years and the 30-year flood levels are presented in Fig. 9 and Table 5. All the models for the mid and far-future climates under SSP1-2.6, except for the MPI-ESM1-2-HR and MRI-ESM2-0 (mid-future), show a decrease in 30-year flood levels ranging from – 13.15% to – 1.53%. Future projections under SSP3-7.0 also show a mixed pattern of increases and decreases in the 30-year flood levels with the highest increase and decrease of 6.39% for the near future climate of MPI-ESM1-2-HR and – 24.75% for the far future climate of GFDL-ESM4, respectively. The models manifest more pronounced projected changes in the 30-year flood levels under the high-end warming scenario of SSP5, specifically,

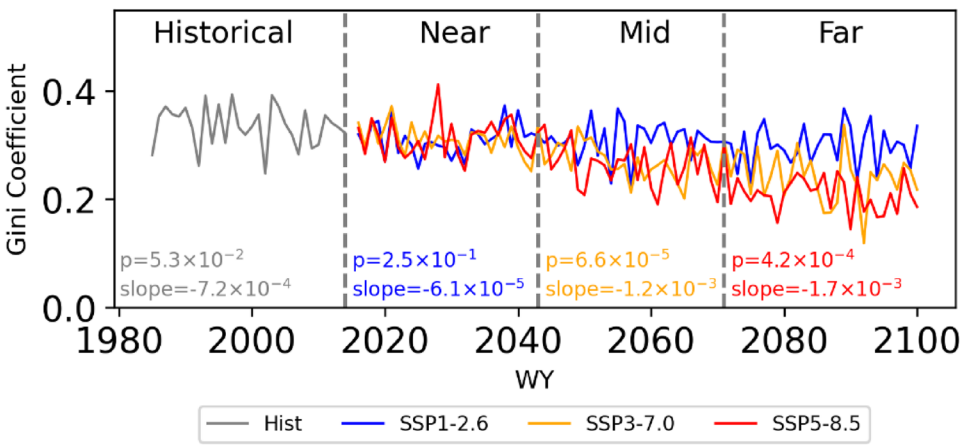

Fig. 8 Future variation of the Gini coefficient relative to the historical period under climate change scenarios

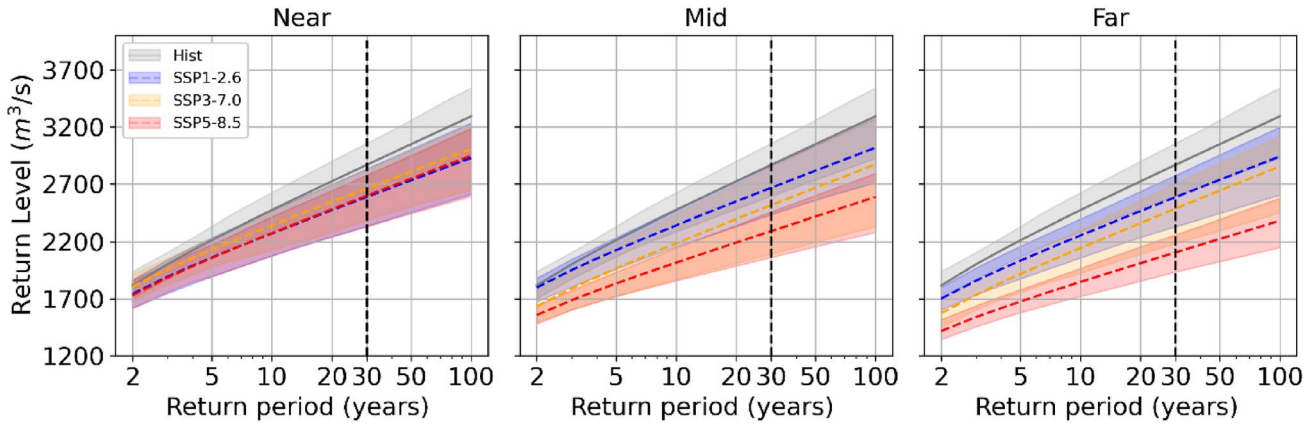

Fig. 9 Flood frequency curves of simulated discharge rates for three future periods relative to the historical period under SSP1-2.6, SSP3-7.0, and SSP5-8.5 based on the Gumbel distribution fit to the annual maxima

Table 5 Projected changes in the 30-year flood levels based on the Gumbel distribution fit to the annual maxima

Scenarios	Datasets	Historical (m^3/s)	Near (m^3/s)	Mid (m^3/s)	Far (m^3/s)	Near-Diff (%)	Mid-Diff (%)	Far-Diff (%)
SSP1-2.6	GFDL	3588	3327	3232	3533	− 7.27	− 9.92	− 1.53
	IPSL	3245	3485	3017	3033	7.40	− 7.03	− 6.53
	MPI	4070	4292	4824	4259	5.45	***18.53***	4.64
	MRI	3705	3887	3707	3263	4.91	0.05	− 11.93
	UKESM	4144	3760	3599	3849	− 9.27	− 13.15	− 7.12
	Ensemble	2868	2589	2667	2585	− 9.73	− 7.01	− 9.87
SSP3-7.0	GFDL	3588	3043	2863	2700	***− 15.19***	***− 20.21***	***− 24.75***
	IPSL	3245	2929	3396	3399	− 9.74	4.65	4.75
	MPI	4070	4330	4205	4268	6.39	3.32	4.86
	MRI	3705	3283	3715	3690	− 11.39	0.27	− 0.40
	UKESM	4144	3888	4277	3939	− 6.18	3.21	− 4.95
	Ensemble	2868	2661	2516	2485	− 7.22	− 12.27	− 13.35
SSP5-8.5	GFDL	3588	3309	2637	2789	− 7.78	***− 26.51***	***− 22.27***
	IPSL	3245	3018	3076	3300	− 7.00	− 5.21	1.69
	MPI	4070	4434	3221	3414	8.94	***− 20.86***	***− 16.12***
	MRI	3705	4064	3388	3373	9.69	− 8.56	− 8.96
	UKESM	4144	3675	3648	3400	− 11.32	− 11.97	***− 17.95***
	Ensemble	2868	2598	2291	2105	− 9.41	***− 20.12***	***− 26.60***

Percentage change of more than ± 15% is shown in bold italic

a decrease of − 26.51% and an increase of 9.69% for the mid-future climate of GFDL-ESM4 and near-future climate of MRI-ESM2-0, respectively.

4.3.2 Variation of extreme flows

For three future climates, the projected changes in the low, medium, and high flows relative to the historical period under the SSP scenarios are shown in Table 6. The Inter-model Ensemble's low flows (P10) will increase in near, mid, and far future climates under all SSP scenarios. In contrast, the high flows (P90) are projected to decrease throughout the twenty-first century under all SSP scenarios, except for the near-future climate under SSP3-7.0 and the mid-future climate under SSP1-2.6. The aforementioned decrement is more pronounced under the high-end warming scenarios of SSPs. Specifically, for the high flows (P90), a decrement of − 18.6% is projected for the far-future climate followed by − 12.4% for the mid-future climate and − 4.8% for the near-future climate under SSP5-8.5. An increase of 16.9%—54.8%

Table 6 Percentage changes in high, medium, and low flows in the Jhelum River basin under SSP1-2.6, SSP3-7.0, and SSP5-8.5

	Climates	Hist (m^3/s)	Change Near-Future (%)			Change Mid-Future (%)			Change Far-Future (%)		
Model	Percentile		SSP1-2.6	SSP3-7.0	SSP5-8.5	SSP1-2.6	SSP3-7.0	SSP5-8.5	SSP1-2.6	SSP3-7.0	SSP5-8.5
Ensemble	P10	287.4	9.9	13.3	11.0	***17.4***	***31.2***	***21.8***	***16.9***	***42.2***	***54.8***
	P25	369.9	12.2	***15.0***	10.6	***15.4***	***30.1***	***23.5***	***17.0***	***40.2***	***46.2***
	P50	620.1	− 1.4	8.0	− 1.0	4.5	10.1	8.1	3.4	14.0	***15.1***
	P75	1134.3	− 2.3	2.8	− 1.7	− 0.3	− 4.6	− 12.9	− 5.3	− 7.6	− 13.3
	P90	1525.9	− 4.0	1.6	− 4.8	1.6	− 7.4	− 12.4	− 2.8	− 8.4	− ***18.6***
GFDL	P10	212.4	11.0	6.8	− 4.6	6.0	***21.1***	4.7	***17.9***	12.2	***15.8***
	P25	321.6	11.5	1.1	− 1.2	3.8	13.2	8.5	9.7	6.9	11.7
	P50	616.6	0.1	− 3.5	− 11.2	− 8.8	− 1.3	− 3.8	− 2.1	− 6.5	− 9.6
	P75	1101.3	0.1	− 9.3	− ***15.9***	− 10.2	− 12.8	− ***16.7***	− 0.7	− ***15.9***	− ***22.3***
	P90	1610.9	− 6.3	− 11.5	− ***15.2***	− 6.8	− 14.4	− ***18.5***	− 0.1	− ***22.6***	− ***25.1***
IPSL	P10	218.6	10.0	***19.3***	14.7	***24.1***	***15.2***	***18.0***	***25.3***	14.2	***31.8***
	P25	344.9	10.6	***15.4***	8.9	12.4	7.4	8.7	***17.7***	1.2	14.7
	P50	597.5	4.5	9.8	4.7	8.8	− 2.5	− 0.5	6.6	− 6.7	− 3.0
	P75	1052.9	− 5.6	− 0.1	− 3.9	− 1.0	− 10.8	− 11.2	− 3.0	− 12.3	− ***15.6***
	P90	1498.3	− 4.9	2.1	− 2.2	0.5	− 8.7	− 6.8	− 4.4	− 10.6	− 14.3
MPI	P10	221.4	***19.1***	***22.7***	12.1	***33.7***	***39.7***	***36.2***	***20.0***	***62.9***	***73.1***
	P25	326.9	12.9	***28.9***	11.9	***24.9***	***35.5***	***35.3***	***19.8***	***51.4***	***64.5***
	P50	596.6	7.2	***20.2***	5.4	13.6	***18.1***	***18.3***	11.1	***28.1***	***29.2***
	P75	1130.5	1.6	***24.1***	6.5	***18.4***	12.0	1.0	1.4	6.8	2.6
	P90	1739.4	5.8	14.1	3.8	***18.2***	7.1	− 9.0	3.0	0.2	− 4.6
MRI	P10	226.7	− 0.2	5.2	3.6	2.9	12.2	5.6	− 0.1	10.8	***25.3***
	P25	342.9	− 4.8	3.2	3.4	− 1.6	6.4	2.6	0.5	13.1	***25.7***
	P50	597.3	− 3.7	7.6	2.6	− 1.1	1.5	− 2.8	− 2.0	9.5	9.0
	P75	1044.7	2.1	9.1	7.2	4.2	5.7	− 2.3	3.0	1.6	− 0.6
	P90	1558.4	4.4	1.3	9.2	4.3	4.9	− 2.8	0.1	5.8	− 5.4
UKESM	P10	221.8	0.8	13.7	***18.6***	***25.2***	***46.2***	***29.2***	***15.0***	***74.0***	***63.6***
	P25	340.2	0.7	8.2	11.1	***24.7***	***37.0***	***26.0***	7.6	***55.5***	***54.9***
	P50	575.5	− 2.5	7.5	7.5	11.1	***22.0***	***16.1***	1.2	***31.9***	***34.5***
	P75	1043.9	− 3.4	1.0	1.1	− 3.6	8.5	− 2.2	− 3.8	13.7	4.3
	P90	1608.8	− 1.0	1.5	− 1.2	− 3.5	6.8	− 2.0	− 0.5	7.4	− 6.4

Percentage change of more than ± 15% is shown in bold italic. P10/ P25/ P50/ P75/ P90 denote percentile values

and 3.4%—15.1% in low (P10 and P25) and median flows (P50) respectively were projected under SSP scenarios for the far-future climate. The median flows (P50) are projected to increase except for the near-future climate under SSP1-2.6 and SSP5-8.5 scenarios. The decline in the high flows indicates that the JRB will face a reduction in future water availability. Future projection uncertainties and constraints are primarily caused by the input data, the internal climatic variability, and the dynamics and parametrization of the climate and hydrological models. The maximum increase of 74.0% in the low flows (P10) is projected for the UKESM far-future climate under the SSP3-7.0 scenario followed by 73.1% for the MPI far-future climate under the SSP5-8.5 scenario, 31.8% for the IPSL far-future climate under the SSP5-8.5 scenario, 25.3% for the MRI far-future climate under the SSP5-8.5 scenario, and 21.1% for the GFDL mid-future climate under the SSP3-7.0 scenario. The maximum decrease in the high flows (P90) is projected for the high-end warming scenario of SSP5-8.5, specifically, − 25.1% followed by − 14.3%, − 9.0, − 6.4%, and − 5.4%, for the GFDL far-future, IPSL far-future, MPI mid-future, UKESM far-future, and MRI far-future climates, respectively.

The trend analysis of the low (P10 and P25) medium (P50) and high (P75 and P90) flows is shown in Table 7. Significant rising (falling) trends were observed for the low (high) flows specifically for the MPI, MRI, and UKESM (for the GFDL and MRI) for the future climate under the SSP5-8.5 scenario. Overall, the ensemble-mean projected flows show a significant rising trend for the P10 (2.35 m^3s^{-1}), P25 (2.41 m^3s^{-1}), and P50 (1.84 m^3s^{-1}) for the far future climate under SSP5-8.5 scenario.

Table 7 Summary of the low, medium, and high flow trends

ESMs-Climate	P10	P25	P50	P75	P90
GFDL-Hist	– 0.57	– 1.43	– 6.70	– 7.67	– 13.99
IPSL-Hist	1.92	***4.72***	6.62	7.62	17.67
MPI-Hist	***3.23***	2.91	3.68	4.22	2.18
MRI-Hist	– 0.04	0.01	2.59	2.69	0.87
UKESM-Hist	0.28	0.03	– 0.75	– 2.50	– 1.86
Ens-Hist	0.65	0.85	2.77	– 1.35	0.35
GFDL-Fut (SSP1-2.6)	0.08	0.21	0.49	– 0.31	1.48
IPSL-Fut (SSP1-2.6)	0.36	0.59	0.20	0.42	– 0.36
MPI-Fut (SSP1-2.6)	0.53	0.21	0.005	0.52	– 0.84
MRI-Fut (SSP1-2.6)	0.51	0.63	0.53	0.92	1.98
UKESM-Fut (SSP1-2.6)	0.30	0.39	0.61	1.49	1.73
Ens-Fut (SSP1-2.6)	0.26	0.33	0.49	0.23	1.57
GFDL-Fut (SSP3-7.0)	0.37	0.29	– 0.09	– 1.85	– 2.45
IPSL-Fut (SSP3-7.0)	– 0.31	– 0.42	– ***1.57***	– ***2.87***	– ***4.74***
MPI-Fut (SSP3-7.0)	***1.71***	1.72	1.42	– 3.32	– 4.36
MRI-Fut (SSP3-7.0)	0.46	0.29	0.52	– 1.01	– 2.34
UKESM-Fut (SSP3-7.0)	***2.66***	***3.40***	***2.76***	1.68	1.44
Ens-Fut (SSP3-7.0)	***1.61***	***1.61***	***1.18***	– 1.84	– 3.17
GFDL-Fut (SSP5-8.5)	0.83	0.86	0.63	– ***2.21***	– 3.29
IPSL-Fut (SSP5-8.5)	0.75	0.59	– 0.45	– 2.32	– 2.82
MPI-Fut (SSP5-8.5)	***2.90***	***3.57***	***3.36***	0.70	0.19
MRI-Fut (SSP5-8.5)	***1.01***	***1.63***	1.32	– 1.50	– ***4.85***
UKESM-Fut (SSP5-8.5)	***2.04***	***2.44***	***2.78***	0.33	– 0.31
Ens-Fut (SSP5-8.5)	***2.35***	***2.41***	***1.84***	– 1.52	– 3.16

Hist and Fut represent historical (1985–2014) and future (2016–2100) climates, respectively. Slopes (m^3s^{-1}) significant at the 95% level are given in bold italic. P10/ P25/ P50/ P75/ P90 denote percentile values

5 Discussions

The eco-hydrological model SWIM employed in this study was calibrated/validated using the meteorological forcing of the observational dataset W5E5. The 5 CMIP6 GCMs used in this study were bias-adjusted to the W5E5 dataset within the Inter-Sectoral Impact Model Intercomparison Project (ISIMIP) phase 3b. Based on the model performance evaluation we observed that the model reproduces the observed discharge with reasonable accuracy but the performance was relatively lower during the validation period. The lower performance during the validation period is due to the coarse resolution of the observed climate data. To resolve the fine-scale hydro-meteorological processes and improve the model evaluation, high-resolution datasets are required.

The climatic projections for the twenty-first century showed a significant increase in Tmax and Tmin [24]. A study conducted by Mahmood et al. [66] also reported a significant increase in future mean annual temperature for A2 and B2 scenarios of HadCM3. Compared to other regions of the country, Pakistan's higher mountainous regions experience a greater rise in temperatures [67]. Saddique et al. [68] reported increasing precipitation trends in the JRB towards the end of the twenty-first century. Munawar et al. [14] also reported an increase of about 2–7% in mean annual precipitation for the twenty-first century. A study conducted by Hartmann and Buchanan [69] reported significantly increasing trends in extreme precipitation in the eastern and northern mountainous regions while significantly decreasing trends in the western Indus River Basin. A study by Yaseen et al. [71] in the Upper Indus River Basin reported increasing and decreasing trends for winter and summer streamflows respectively. Snowmelt has a noticeable impact on streamflow in the Jhelum River basin, where almost 65% of the catchment is covered in snow at the end of the winter season [72]. Rizwan et al. [17] also reported a decrease in the magnitude of peak discharge for the JRB. Ahmad et al. [74] reported falling trends in annual runoff volumes (1978–2005) for the Jhelum River at Azad Pattan. Rizwan et al. [17] also reported a decrease in the projected streamflow for the near (2020–2059) and

far (2060–2099) future climates for five GCMs (BCC-CSM1-1, GFDL-ESM2M, IPSL-CM5A-LR, IPSL-CM5A-MR, and MPI-ESM-LR) under three RCP (RCP 2.6, RCP 4.5, and RCP 8.5) scenarios. A study by Babur et al. [29] reported a decrease in the future average annual discharge for the near-, mid-, and far-future climates for one GCM (CCSM4). In contrast, an increase was observed for four GCMs (MRICGM3, MIROC5, CSIRO BOM ACCESS1-0, and GFDL-CM3) under RCP 4.5 and RCP 8.5 scenarios. A study carried out in the JRB reported discharge fluctuations tend to rise during the winter and spring seasons while falling during the summer and autumn [29]. The occurrence of precipitation in the form of rain (liquid precipitation) during winter and the increased contribution of snowmelt to the runoff in the basin are the likely causes of the increased streamflow during the winter and spring [78]. According to a study conducted by Khattak et al. [75], the streamflow at Besham, a hydrometric station upstream of Tarbela Reservoir, increased in the winter and spring and decreased in the summer. Several studies conducted in the JRB reported that the average annual stream flow in future climates could decline [16, 17]. Mahmood and Jia [79] found decreasing trends for summer flows while increasing trends for winter flows in the JRB at Azad Pattan. Shafiq et al. [80] reported significantly decreasing streamflow trends for all stations of JRB and the decrease was more pronounced during spring and summer. Saddique et al. [13] found an increasing trend for winter and autumn while for summer and spring, the trends were inconsistent. Khattak et al. [81] reported increasing trends for winter and spring flows at Mangla while decreasing trends during summer. The studies conducted in the JRB by Jasrotia et al. [82] and Munawar et al. [14] also reported a declining trend in the runoff during the last two decades of the twenty-first century.

Lehner et al. [83] reported the emergence of observed temperature changes in both winter and summer in the northern extratropics. Nguyen et al. [84] used several climate models from the Coupled Model Intercomparison Project phase 5 (CMIP5) to perform an updated Time of Emergence (ToE) analysis of regional precipitation changes over 14 precipitation change hotspots worldwide. Another study conducted across China studied the precipitation and flow regimes using GC and reported that temporally the flow regimes manifest increasing homogenization [89]. Masaki et al. [90] performed a global study to analyze the characteristics of GC to understand the changes in future flow regimes of major rivers and found a declining seasonal inequality at high northern latitudes.

The ISIMIP dataset utilized in this study was previously employed in the study conducted by Gädeke et al. [18] to analyze peak flow magnitude. In their study, they also employed the eco-hydrological model SWIM to simulate the hydrological cycle of the Ganges, Brahmaputra, and Meghna basins at a daily time step. The authors reported that the recurrence intervals of Qmax exhibit a strong agreement between the observed datasets and hydrological model simulations driven by the observed climate of W5E5 and simulations forced by the historical CMIP datasets.

A study based on the flood frequency analysis conducted by Zakaullah et al. [91] reported that Gumbel distribution is best for the JRB. Another study by Ahsan et al. [92] also reported that Gumbel distribution is the best fit for the Indus and Jhelum River basins. Several other studies in Pakistan also reported Gumbel distribution as a best fit. For instance, Boota et al. [93] studied Probable Maximum Precipitation in the mountainous regions of Pakistan and found the Gumbel distribution as best. Ijaz et al. [94] performed a Chenab River flood frequency analysis and reported the Gumbel distribution as the most appropriate. Haider and Massod [95] performed flood frequency analysis in the Upper Indus Basin and reported that the Gumbel distribution is best for predicting river flow. Naz et al. [96] applied Gumbel distribution to study the flood risk assessment of the Indus River at Guddu Barrage. Faisal et al. [97] found that Gumbel distribution is suitable for predicting streamflows of Nullah Deg located in Northeast Punjab Pakistan.

An overall increase (decrease) in the low (high) flows is in line with the findings of Mahmood and Jia [12]. A study by Yaseen et al. [98] reported a decrease in the magnitude of annual maximum/high flows for the JRB.

The present study has several limitations. For example, throughout the simulated periods, the land cover and soil characteristics remained unchanged, which may have an impact on the basin's streamflow projections. GCMs owing to their coarse spatial resolution have the limited ability to capture small-scale watershed processes. Another limitation is the short duration of observed discharge for model calibration and validation. Researchers can improve the accuracy and robustness of streamflow estimates for the management of water resources by addressing these limitations.

6 Conclusions

The impacts of climate change on the streamflow regime of the JRB by forcing the eco-hydrological model SWIM with five ESMs under SSP1-2.6, SSP3-7.0, and SSP5-8.5 scenarios, for the historical (1985–2014) and three future periods defined as near (2016–2043), mid (2044–2071), and far (2072–2100) were investigated. Based on the model evaluation criteria, the calibrated/validated model adequately replicated the observed discharge in the JRB and accurately represented the

hydrological processes of the basin. All ESMs indicated that the mean temperature would rise over the century under all SSP scenarios. The findings also indicate that precipitation will increase in the future period. Streamflows were projected to decrease during summer and increase during winter compared to the historical period. The analysis regarding the time of emergence of streamflow revealed an earlier emergence of future low flows as compared to the high flows. The GC results showed a pattern of increasing homogenization of future streamflows under all SSP scenarios. Flood frequency analysis revealed a decrease in 30-year flood levels implying that the severity of such events is expected to be lower in the future. Under all SSP scenarios, the high flows will mostly decrease, while low flows will rise in the near, mid, and far future climates relative to the historical period. The findings of this study will advance our knowledge of the climate change impacts on future discharge and serve as a guide for developing future watershed water resource management policies.

7 Recommendations

For Future research, the main recommendations are as follows:

Focus on improving the spatial resolution of the climate models to capture regional and local climate variations more accurately.

Enhanced representation of land-surface processes and their interactions with atmospheric conditions.

Employing more than one hydrological model to analyze the range of possible outcomes and to identify the degree of uncertainty in streamflow projections.

Utilizing fully distributed hydrological models for effective water management and environmental decision-making in diverse and complex landscapes.

Author contributions MJ: data curation, conceptualization, methodology, hydrological modelling, analysis, and original draft write-up; JB: conceptualization, investigation, review, and editing; SH: conceptualization, methodology, original draft write-up. All authors read and approved the final manuscript.

Funding Open Access funding enabled and organized by Projekt DEAL. The authors acknowledge the support from the Deutsche Forschungsgemeinschaft (DFG, German Research Foundation) under Germany's Excellence Strategy-EXC 2037 "CLICCS-Climate, Climatic Change, and Society"-Project Number: 390683824, contribution to the Center for Earth System Research and Sustainability (CEN) of Universität Hamburg. We acknowledge financial support from the Open Access Publication Fund of Universität Hamburg.

Data availability The data used in this research are available by the corresponding author upon reasonable request.

Declarations

Ethics approval and consent to participate The authors confirm that this article is original research and has not been published or presented previously in any journal or conference in any language (in whole or in part).

Consent to publication All authors read and approved the final manuscript.

Competing interests The authors declare no competing interests.

References

1. Stocker TF, Qin D, Plattner GK, Tignor MM, Allen SK, Boschung J, Nauels A, Xia Y, Bex V, Midgley PM. Climate Change 2013 The physical science basis contribution of working group I to the fifth assessment report of IPCC the intergovernmental panel on climate change. London: Cambridge University Press; 2014.

2. Kundzewicz ZW. Climate change impacts on the hydrological cycle. Ecohydrol Hydrobiol. 2008;8(2–4):195–203. https://doi.org/10.2478/v10104-009-0015-y.
3. Ma J, Zhou L, Foltz GR, Qu X, Ying J, Tokinaga H, Mechoso CR, Li J, Gu X. Hydrological cycle changes under global warming and their effects on multiscale climate variability. Ann N Y Acad Sci. 2020;1472(1):21–48. https://doi.org/10.1111/nyas.14335.
4. Zhang Y, You Q, Chen C, Ge J. Impacts of climate change on streamflows under RCP scenarios: a case study in Xin River Basin China. Atmos Res. 2016;178:521–34. https://doi.org/10.1016/j.atmosres.2016.04.018.
5. Bajracharya AR, Bajracharya SR, Shrestha AB, Maharjan SB. Climate change impact assessment on the hydrological regime of the Kaligandaki Basin Nepal. Sci Total Environ. 2018;625:837–48. https://doi.org/10.1016/j.scitotenv.2017.12.332.
6. Gashaw T, Wubaye GB, Worqlul AW, Dile YT, Mohammed JA, Birhan DA, Tefera GW, van Oel PR, Haileslassie A, Chukalla AD, Taye MT. Local and regional climate trends and variabilities in Ethiopia: Implications for climate change adaptations. Environ Chall. 2023;13: 100794. https://doi.org/10.1016/j.envc.2023.100794.
7. Schoof JT, Robeson SM. Projecting changes in regional temperature and precipitation extremes in the United States. Weather Climate Extremes. 2016;11:28–40. https://doi.org/10.1016/j.wace.2015.09.004.
8. Ahmad S. Change in glaciers length in the Indian Himalaya: an observation and prediction under warming scenario. Model Earth Syst Environ. 2016;2:1. https://doi.org/10.1007/s40808-016-0221-8.
9. Dahal N, Shrestha UB, Tuitui A, Ojha HR. Temporal changes in precipitation and temperature and their implications on the streamflow of Rosi River, Central Nepal. Climate. 2018;7(1):3. https://doi.org/10.3390/cli7010003.
10. Lehner F, Wood AW, Vano JA, Lawrence DM, Clark MP, Mankin JS. The potential to reduce uncertainty in regional runoff projections from climate models. Nat Clim Chang. 2019;9(12):926–33. https://doi.org/10.1038/s41558-019-0639-x.
11. Tan X, Gan TY. Contribution of human and climate change impacts to changes in streamflow of Canada. Sci Rep. 2015;5(1):17767. https://doi.org/10.1038/srep17767.
12. Mahmood R, Jia S. Assessment of impacts of climate change on the water resources of the transboundary Jhelum River basin of Pakistan and India. Water. 2016;8(6):246. https://doi.org/10.3390/W8060246.
13. Saddique N, Usman M, Bernhofer C. Simulating the impact of climate change on the hydrological regimes of a sparsely gauged mountainous basin, Northern Pakistan. Water. 2019;11(10):2141. https://doi.org/10.3390/w11102141.
14. Munawar S, Tahir MN, Baig MH. Future climate change impacts on runoff of scarcely gauged Jhelum river basin using SDSM and RCPs. J Water Climate Change. 2021;12(7):2993–3004. https://doi.org/10.2166/wcc.2021.283.
15. Azmat M, Qamar MU, Huggel C, Hussain E. Future climate and cryosphere impacts on the hydrology of a scarcely gauged catchment on the Jhelum river basin, Northern Pakistan. Sci Total Environ. 2018;639:961–76. https://doi.org/10.1016/j.scitotenv.2018.05.206.
16. Ahsan S, Bhat MS, Alam A, Farooq H, Shiekh HA. Complementary use of multi-model climate ensemble and Bayesian model averaging for projecting river hydrology in the Himalaya. Environ Sci Pollut Res. 2023;30(13):38898–920. https://doi.org/10.1007/s11356-022-24913-6.
17. Rizwan M, Li X, Chen Y, Anjum L, Hamid S, Yamin M, Chauhdary JN, Shahid MA, Mehmood Q. Simulating future flood risks under climate change in the source region of the Indus River. J Flood Risk Manag. 2023;16(1): e12857. https://doi.org/10.1111/jfr3.12857.
18. Gädeke A, Wortmann M, Menz C, Islam AS, Masood M, Krysanova V, Lange S, Hattermann FF. Climate impact emergence and flood peak synchronization projections in the Ganges, Brahmaputra and Meghna basins under CMIP5 and CMIP6 scenarios. Environ Res Lett. 2022;17(9): 094036. https://doi.org/10.1088/1748-9326/ac8ca1.
19 Her Y, Yoo SH, Cho J, Hwang S, Jeong J, Seong C. Uncertainty in hydrological analysis of climate change: multi-parameter vs. multi-GCM ensemble predictions. Sci Rep. 2019;9(1):4974. https://doi.org/10.1038/s41598-019-41334-7.
20. Ahmadalipour A, Rana A, Moradkhani H, Sharma A. Multi-criteria evaluation of CMIP5 GCMs for climate change impact analysis. Theoret Appl Climatol. 2017;128:71–87. https://doi.org/10.1007/s00704-015-1695-4.
21. Wilby RL, Hay LE, Gutowski WJ Jr, Arritt RW, Takle ES, Pan Z, Leavesley GH, Clark MP. Hydrological responses to dynamically and statistically downscaled climate model output. Geophys Res Lett. 2000;27(8):1199–202. https://doi.org/10.1029/1999GL006078.
22. Mishra Y, Nakamura T, Babel MS, Ninsawat S, Ochi S. Impact of climate change on water resources of the Bheri River Basin. Nepal Water. 2018;10(2):220. https://doi.org/10.3390/w10020220.
23. Barron EJ. Beyond climate science. Science. 2009. https://doi.org/10.1126/science.11798.
24. Munawar S, Rahman G, Moazzam MF, Miandad M, Ullah K, Al-Ansari N, Linh NT. Future climate projections using SDSM and LARS-WG downscaling methods for CMIP5 GCMs over the transboundary Jhelum River Basin of the Himalayas Region. Atmosphere. 2022;13(6):898. https://doi.org/10.3390/atmos13060898.
25. Saddique N, Mahmood T, Bernhofer C. Quantifying the impacts of land use/land cover change on the water balance in the afforested River Basin, Pakistan. Environ Earth Sci. 2020;79(19):448. https://doi.org/10.1007/s12665-020-09206-w.
26. Hasson S, Pascale S, Lucarini V, Böhner J. Seasonal cycle of precipitation over major river basins in South and Southeast Asia: a review of the CMIP5 climate models data for present climate and future climate projections. Atmos Res. 2016;180:42–63. https://doi.org/10.1016/j.atmosres.2016.05.008.
27. Saddique N, Bernhofer C, Kronenberg R, Usman M. Downscaling of CMIP5 models output by using statistical models in a data scarce mountain environment (Mangla Dam Watershed), Northern Pakistan. Asia-Pac J Atmos Sci. 2019;55:719–35. https://doi.org/10.1007/s13143-019-00111-2.
28. Hasson S, Lucarini V, Khan MR, Petitta M, Bolch T, Gioli G. Early 21st century snow cover state over the western river basins of the Indus River system. Hydrol Earth Syst Sci. 2014;18(10):4077–100. https://doi.org/10.5194/hess-18-4077-2014.
29. Babur M, Babel MS, Shrestha S, Kawasaki A, Tripathi NK. Assessment of climate change impact on reservoir inflows using multi climate-models under RCPs—The case of Mangla Dam in Pakistan. Water. 2016;8(9):389. https://doi.org/10.3390/w8090389.
30. Archer DR, Fowler HJ. Using meteorological data to forecast seasonal runoff on the River Jhelum Pakistan. J Hydrol. 2008;361(1–2):10–23. https://doi.org/10.1016/j.jhydrol.2008.07.017.
31. Cucchi M, Weedon GP, Amici A, Bellouin N, Lange S, Müller Schmied H, Hersbach H, Buontempo C. WFDE5: bias-adjusted ERA5 reanalysis data for impact studies. Earth Syst Sci Data. 2020;12(3):2097–120. https://doi.org/10.5194/essd-12-2097-2020.
32. Lange S. ISIMIP3b bias adjustment fact sheet. Potsdam: Inter-Sectoral Impact Model Intercomparison Project. 2021. https://doi.org/10.5281/ZENODO.4686991.

33 Lange S. Trend-preserving bias adjustment and statistical downscaling with ISIMIP3BASD (v1. 0). Geosci Model Dev. 2019;12(7):3055–70. https://doi.org/10.5194/gmd-12-3055-2019.
34. Lange S, Menz C, Gleixner S, Cucchi M, Weedon GP, Amici A, Bellouin N, Schmied HM, Hersbach H, Buontempo C, Cagnazzo C. WFDE5 over land merged with ERA5 over the ocean (W5E5 v2. 0). https://doi.org/10.48364/ISIMIP.342217
35. Farr TG, Rosen PA, Caro E, Crippen R, Duren R, Hensley S, Kobrick M, Paller M, Rodriguez E, Roth L, Seal D. The shuttle radar topography mission. Rev Geophys. 2007. https://doi.org/10.1029/2005RG000183.
36. Fischer G, Nachtergaele F, Prieler S, Van Velthuizen HT, Verelst L, Wiberg D. Global agro-ecological zones assessment for agriculture (GAEZ 2008). IIASA, Laxenburg, Austria and FAO, Rome, Italy. 2008.
37. Arino O, Ramos Perez J, Kalogirou V, Bontemps S, Defourny P, van Bogaert, E. Global Land Cover Map for 2009 (GlobCover 2009); European Space Agency (ESA) & Université Catholique de Louvain (UCL): Frascati, Italy. 2012. https://doi.org/10.1594/PANGAEA.787668.
38. Li Y, Li F, Shangguan D, Ding Y. A new global gridded glacier dataset based on the Randolph Glacier Inventory version 6.0. J Glaciol. 2021;67(264):773–6. https://doi.org/10.1017/jog.2021.28.
39. Farinotti D, Huss M, Fürst JJ, Landmann J, Machguth H, Maussion F, Pandit A. A consensus estimate for the ice thickness distribution of all glaciers on Earth. Nat Geosci. 2019;12(3):168–73. https://doi.org/10.1038/s41561-019-0300-3.
40. Kriegler E, O'Neill BC, Hallegatte S, Kram T, Lempert RJ, Moss RH, Wilbanks T. The need for and use of socio-economic scenarios for climate change analysis: a new approach based on shared socio-economic pathways. Glob Environ Chang. 2012;22(4):807–22. https://doi.org/10.1016/j.gloenvcha.2012.05.005.
41. O'Neill BC, Carter T, Ebi KL, Edmonds J, Hallegatte S, Kemp-Benedict E, Kriegler E, Mearns L, Moss R, Riahi K, van Ruijven B. Meeting report of the workshop on the nature and use of new socioeconomic pathways for climate change research. HAL; 2012.
42. Meinshausen M, Nicholls ZR, Lewis J, Gidden MJ, Vogel E, Freund M, Beyerle U, Gessner C, Nauels A, Bauer N, Canadell JG. The shared socio-economic pathway (SSP) greenhouse gas concentrations and their extensions to 2500. Geosci Model Dev. 2020;13(8):3571–605. https://doi.org/10.5194/gmd-13-3571-2020.
43. Kendall MG. Rank Correlation Methods. Griffin London, UK. 1975.
44. Mann HB. Nonparametric tests against trend. Econometrica: Journal of the econometric society. 1945. 245:59.
45. Sen PK. Estimates of the regression coefficient based on Kendall's tau. J Am Stat Assoc. 1968;63(324):1379–89. https://doi.org/10.2307/2285891.
46. Theil H. A rank-invariant method of linear and polynomial regression analysis, I, II, III. In Henri Theil's Contributions to Economics and Econometrics. Springer Amsterdam, The Netherlands. 1992; pp. 386–392, 512–525, 1397–1412.
47 Tabari H, Hosseinzadeh TP. Recent trends of mean maximum and minimum air temperatures in the western half of Iran. Meteorol Atmos Phys. 2011. https://doi.org/10.1007/s00703-011-0125-0.
48. Bocchiola D, Diolaiuti G. Recent (1980–2009) evidence of climate change in the upper Karakoram Pakistan. Theoret Appl Climatol. 2013;113:611–41. https://doi.org/10.1007/s00704-012-0803-y.
49. Hasson S, Böhner J, Lucarini V. Prevailing climatic trends and runoff response from Hindukush–Karakoram–Himalaya, upper Indus Basin. Earth System Dynamics. 2017;8(2):337–55. https://doi.org/10.5194/esd-8-337-2017.
50. Karki R, Hasson SU, Schickhoff U, Scholten T, Böhner J. Rising precipitation extremes across Nepal. Climate. 2017;5(1):4. https://doi.org/10.3390/cli5010004.
51. Yue S, Wang CY. Applicability of prewhitening to eliminate the influence of serial correlation on the Mann-Kendall test. Water Resour Res. 2002;38(6):4–1. https://doi.org/10.1029/2001wr000861.
52 Moriasi DN, Gitau MW, Pai N, Daggupati P. Hydrologic and water quality models: Performance measures and evaluation criteria. Trans ASABE. 2015;58(6):1763–85. https://doi.org/10.13031/trans.58.10715.
53. Collins DB. Hydrological sentinels and the relative emergence of climate change signals in New Zealand river flows. Hydrol Sci J. 2021;66(15):2146–54. https://doi.org/10.1080/02626667.2021.1987439.
54. King AD, Donat MG, Fischer EM, Hawkins E, Alexander LV, Karoly DJ, Dittus AJ, Lewis SC, Perkins SE. The timing of anthropogenic emergence in simulated climate extremes. Environ Res Lett. 2015;10(9): 094015. https://doi.org/10.1088/1748-9326/10/9/094015.
55 Giorgi F, Bi X. Time of emergence (TOE) of GHG-forced precipitation change hot-spots. Geophys Res Lett. 2009. https://doi.org/10.1029/2009GL037593.
56. Mahlstein I, Knutti R, Solomon S, Portmann RW. Early onset of significant local warming in low latitude countries. Environ Res Lett. 2011;6(3): 034009. https://doi.org/10.1088/1748-9326/6/3/034009.
57 Mahlstein I, Hegerl G, Solomon S. Emerging local warming signals in observational data. Geophys Res Lett. 2012. https://doi.org/10.1029/2012GL053952.
58 Hawkins E, Sutton R. Time of emergence of climate signals. Geophys Res Lett. 2012. https://doi.org/10.1029/2011GL050087.
59. John A, Nathan R, Horne A, Fowler K, Stewardson M, Peel M, Webb JA. The time of emergence of climate-induced hydrologic change in Australian rivers. J Hydrol. 2023;619: 129371. https://doi.org/10.1016/j.jhydrol.2023.129371.
60. Muelchi R, Rössler O, Schwanbeck J, Weingartner R, Martius O. River runoff in Switzerland in a changing climate–runoff regime changes and their time of emergence. Hydrol Earth Syst Sci. 2021;25(6):3071–86. https://doi.org/10.5194/hess-25-3071-2021.
61 Jawitz JW, Mitchell J. Temporal inequality in catchment discharge and solute export. Water Resourc Res. 2011. https://doi.org/10.1029/2010WR010197.
62. Gumbel EJ. The return period of flood flows. Ann Math Stat. 1941;12(2):163–90.
63 Gumbel EJ. Statistics of extremes. London: Columbia University Press. 1958.
64. Ahad U, Ali U, Inayatullah M, Rauf SA. Flood frequency analysis: a case study of Pohru river catchment, Kashmir Himalayas, India. J Geol Soc India. 2022;98(12):1754–60. https://doi.org/10.1007/s12594-022-2247-z.
65. Bhat MS, Alam A, Ahmad B, Kotlia BS, Farooq H, Taloor AK, Ahmad S. Flood frequency analysis of river Jhelum in Kashmir basin. Quatern Int. 2019;507:288–94. https://doi.org/10.1016/j.quaint.2018.09.039.
66. Mahmood R, Babel MS, Shaofeng JI. Assessment of temporal and spatial changes of future climate in the Jhelum river basin, Pakistan and India. Weather Climate Extremes. 2015;10:40–55. https://doi.org/10.1016/j.wace.2015.07.002.

67. Kazmi DH, Li J, Rasul G, Tong J, Ali G, Cheema SB, Liu L, Gemmer M, Fischer T. Statistical downscaling and future scenario generation of temperatures for Pakistan Region. Theoret Appl Climatol. 2015;120:341–50. https://doi.org/10.1007/s00704-014-1176-1.
68. Saddique N, Khaliq A, Bernhofer C. Trends in temperature and precipitation extremes in historical (1961–1990) and projected (2061–2090) periods in a data scarce mountain basin, northern Pakistan. Stoch Env Res Risk Assess. 2020;34:1441–55. https://doi.org/10.1007/s00477-020-01829-6.
69. Hartmann H, Buchanan H. Trends in extreme precipitation events in the Indus River Basin and flooding in Pakistan. Atmos Ocean. 2014;52(1):77–91. https://doi.org/10.1080/07055900.2013.859124.
70. Ali S, Kim BH, Akhtar T, Kam J. Past and future changes toward earlier timing of streamflow over Pakistan from bias-corrected regional climate projections (1962–2099). J Hydrol. 2023;617: 128959. https://doi.org/10.1016/j.jhydrol.2022.128959.
71. Yaseen M, Ahmad I, Guo J, Azam MI, Latif Y. Spatiotemporal variability in the hydrometeorological time-series over upper Indus river basin of Pakistan. Adv Meteorol. 2020;2020(1):5852760. https://doi.org/10.1155/2020/5852760.
72. Azmat M, Choi M, Kim TW, Liaqat UW. Hydrological modeling to simulate streamflow under changing climate in a scarcely gauged cryosphere catchment. Environ Earth Sci. 2016;75:1–6. https://doi.org/10.1007/s12665-015-5059-2.
73 Hanus S, Hrachowitz M, Zekollari H, Schoups G, Vizcaino M, Kaitna R. Future changes in annual, seasonal and monthly runoff signatures in contrasting Alpine catchments in Austria. Hydrology and Earth System Sciences. 2021;25(6):3429-53. https://doi.org/10.5194/hess-25-3429-2021.
74. Ahmad Z, Hafeez M, Ahmad I. Hydrology of mountainous areas in the upper Indus Basin, Northern Pakistan with the perspective of climate change. Environ Monit Assess. 2012;184:5255–74. https://doi.org/10.1007/s10661-011-2337-7.
75. Khattak MS, Babel MS, Sharif M. Hydro-meteorological trends in the upper Indus River basin in Pakistan. Climate Res. 2011;46(2):103–19. https://doi.org/10.3354/cr00957.
76. Han J, Liu Z, Woods R, McVicar TR, Yang D, Wang T, Hou Y, Guo Y, Li C, Yang Y. Streamflow seasonality in a snow-dwindling world. Nature. 2024;629(8014):1075–81. https://doi.org/10.1038/s41586-024-07299-y.
77. Sharma V, Mishra VD, Joshi PK. Implications of climate change on streamflow of a snow-fed river system of the Northwest Himalaya. J Mt Sci. 2013;10(4):574–87. https://doi.org/10.1007/s11629-013-2667-8.
78. Romshoo SA, Marazi A. Impact of climate change on snow precipitation and streamflow in the Upper Indus Basin ending twenty-first century. Clim Change. 2022;170(1):6. https://doi.org/10.1007/s10584-021-03297-5.
79. Mahmood R, Jia S. Spatial and temporal hydro-climatic trends in the transboundary Jhelum River basin. J Water Climate Change. 2017;8(3):423–40. https://doi.org/10.2166/wcc.2017.005.
80. UlShafiq M, Ashraf I, Ul Islam Z, Ahmed P, Dimri AP. Response of streamflow to climate variability in the source region of Jhelum River Basin in Kashmir valley India. Nat Hazards. 2020;104:611–37. https://doi.org/10.1007/s11069-020-04183-6.
81. Khattak MS, Reman NU, Sharif M, Khan MA. Analysis of streamflow data for trend detection on major rivers of the Indus Basin. J Himalayan Earth Sci. 2015;48(1):87.
82. Jasrotia AS, Baru D, Kour R, Ahmad S, Kour K. Hydrological modeling to simulate stream flow under changing climate conditions in Jhelum catchment, western Himalaya. J Hydrol. 2021;1(593): 125887. https://doi.org/10.1016/j.jhydrol.2020.125887.
83. Lehner F, Deser C, Terray L. Toward a new estimate of "time of emergence" of anthropogenic warming: insights from dynamical adjustment and a large initial-condition model ensemble. J Clim. 2017;30(19):7739–56. https://doi.org/10.1175/JCLI-D-16-0792.1.
84. Nguyen TH, Min SK, Paik S, Lee D. Time of emergence in regional precipitation changes: an updated assessment using the CMIP5 multi-model ensemble. Clim Dyn. 2018;51:3179–93. https://doi.org/10.1007/s00382-018-4073-y.
85. Leng G, Huang M, Voisin N, Zhang X, Asrar GR, Leung LR. Emergence of new hydrologic regimes of surface water resources in the conterminous United States under future warming. Environ Res Lett. 2016;11(11): 114003. https://doi.org/10.1088/1748-9326/11/11/114003.
86. Zhuan MJ, Chen J, Shen MX, Xu CY, Chen H, Xiong LH. Timing of human-induced climate change emergence from internal climate variability for hydrological impact studies. Hydrol Res. 2018;49(2):421–37. https://doi.org/10.2166/nh.2018.059.
87. Ye Q, Li Z, Duan L, Xu X. Decoupling the influence of vegetation and climate on intra-annual variability in runoff in karst watersheds. Sci Total Environ. 2022;824: 153874. https://doi.org/10.1016/j.scitotenv.2022.153874.
88. Kuntla SK, Saharia M, Prakash S, Villarini G. Precipitation inequality exacerbates streamflow inequality, but dams moderate it. Sci Total Environ. 2024;912: 169098. https://doi.org/10.1016/j.scitotenv.2023.169098.
89. Zhang Q, Gu X, Singh VP, Xu CY, Kong D, Xiao M, Chen X. Homogenization of precipitation and flow regimes across China: changing properties, causes and implications. J Hydrol. 2015;530:462–75. https://doi.org/10.1016/j.jhydrol.2015.09.041.
90. Masaki Y, Hanasaki N, Takahashi K, Hijioka Y. Global-scale analysis on future changes in flow regimes using Gini and Lorenz asymmetry coefficients. Water Resour Res. 2014;50(5):4054–78. https://doi.org/10.1002/2013WR014266.
91. Zakaullah U, Saeed MM, Ahmad I, Nabi G. Flood frequency analysis of homogeneous regions of Jhelum River Basin. Int J Water Resour Environ Eng. 2012;4:144–9.
92. Ahsan H, Nabi G, Boota MW, Abbas T. Development of envelope curve for Indus and Jhelum River basin in Pakistan and estimation of upper bound using envelope curve. J Himalayan Earth Sci. 2016;49(1):98.
93. Boota MW, Nabi G, Abbas T, Jin H, Yousaf A, Boota MA. Comparative study of probable maximum precipitation and isohyetal maps for mountainous regions, Pakistan. Sci Cold Arid Regions. 2018;10(1):55–68.
94. Ijaz S, Hameed Q, Ahsan A, Butt MA. Flood frequency analysis of Chenab River for predicting peak flows during late monsoon period. Adv Remote Sens. 2019;8(1):1–29. https://doi.org/10.4236/ars.2019.81001.
95. Haider S, Masood MU. Analyzing Frequency of Floods in Upper Indus Basin under Various Climate Change Scenarios. InProceedings of the 2nd National Conference on Sustainable Water Resources Management (SWRM-22), Lahore, Pakistan 2022 Nov 16 (pp. 137–141).
96. Naz S, Baig MJ, Inayatullah S, Siddiqi TA, Ahsanuddin M. Flood risk assessment of Guddu Barrage using Gumbel's distribution. Int J Sci. 2019;8(04):33-8. https://doi.org/10.18483/ijSci.2024.
97. Faisal M, Nabi G, Abbas T, Yaseen M, Boota MW. An appraisal of flood occurrence and Varability in Streamflows of Nullah Deg, north east Punjab, Pakistan.

98. Yaseen M, Latif Y, Waseem M, Leta MK, Abbas S, Akram BH. Contemporary trends in high and low river flows in upper Indus Basin, Pakistan. Water. 2022;14(3):337. https://doi.org/10.3390/w14030337.
99. Krysanova V, Wechsung F, Arnold J, Ragavan S, Williams J. SWIM (Soil and Water Integrated Model), User Manual, Report No. 69. Potsdam (Germany) PIK. 2000.
100. Krysanova V, Meiner A, Roosaare J, Vasilyev A. Simulation modelling of the coastal waters pollution from agricultural watershed. Ecological modelling. 1989;49(1-2):7-29. https://doi.org/10.1016/0304-3800(89)90041-0.